April 2013

Mathematical Model of Chemotactic Signaling in Sea Urchin Sperm

Daniel Michael Duhaney
Worcester Polytechnic Institute

Project Number: MQP-SDO-202

Mathematical Model of Chemotactic Signaling in Sea Urchin Sperm

A Major Qualifying Project

submitted to the Faculty of

Worcester Polytechnic Institute

in partial fulfillment of the requirements for the

Degree of Bachelor of Science

by

Daniel Duhaney

April 23, 2013

Approved:

Prof. Sarah Olson

Abstract

We develop a system of ODEs to model the change in calcium concentration in *A. punctulata* sperm flagella in response to chemotactic signaling. The change in calcium concentration is dependent on membrane voltage, which is in turn dependent on ion channel mechanics. We assume the ion channels can be modeled using Hodgkin-Huxley equations. We numerically solve the system of coupled nonlinear ODEs and present the results for membrane voltage and calcium concentration. Experimental data, parameter estimation, and future plans to use this model to gain insight into sperm movement are discussed.

Executive Summary

Unlike mammalian reproduction, for which fertilization occurs internally, marine animals such as the purple-spined sea urchin release their sperm into the ocean. The sperm cells of the purple-spined sea urchin, Arbacia punctulata, locate the eggs through chemotaxis, biased movement in response to a chemical signal. In summary, the sea urchin egg releases a chemical called resact. Upon contact with the cell, resact induces a signal that results in calcium flux into the sperm tail, which stimulates the oscillations that propel sperm in the direction of the egg. Thus we can understand the chemotactic process by understanding the process behind calcium influx.

To understand calcium influx, it is necessary to investigate the signaling pathway behind the interaction. The signaling pathway comes about from changes in the sperm's membrane potential. Stimulation by resact induces multiple ion currents through membrane channels, bringing about voltage changes due to ions moving in and out of the cell. It is these voltage changes that activate the calcium influx. Thus, to track calcium current, it is necessary to track membrane voltage and the currents of all the channels. The membrane voltage and the actions of the ion channels can be modeled using Hodgkin-Huxley equations, which consider the cell membrane and channels as a circuit and apply Kirchhoff's current law to determine the change in voltage with respect to time.

Using Hodgkin-Huxley equations as a guide, we developed a system of four non-linear differential equations to describe the membrane voltage and ion currents and flux. The activation of one ion channel in particular, the KCNG channel, depends on a second messenger chemical called cGMP to activate and start the pathway. We modeled the dynamics of this chemical in two ways: by interpolating experimental concentration data, and by developing an ODE to describe cGMP dynamics, where the parameters were fitted using optimization in order to match the data.

Putting the equations together, our goal is to understand the pieces of the pathway. We again estimated parameters to get the baseline (unstimulated) case, since literature values for parameters were given in a range or for other species. Running the full model, we were unsuccessful in reproducing expected results from the literature. However, we were able to study the dynamics of currents for several currents and gained an understanding of the coupling of the channel activities and how the gating of channels changes membrane potential.

Acknowledgments

I would like to thank Professor Sarah Olson of the Mathematical Sciences Department for her thoughtful advice and continued patience with me throughout this project.

Contents

List of Figures

List of Tables

Chapter 1

Introduction

Figure 1.1: *Arbacia punctulata*, the purple-spined sea urchin, commonly found along the east coast of the United States and in the Gulf of Mexico (reprinted from [12])

Much of life on Earth is borne from sexual reproduction. This requires a male gamete, also known as a spermatozoon or simply sperm, to locate and fertilize a female gamete, or egg. For this to occur, communication must occur between the male and female gametes. This is especially important for the purple-spined sea urchin *Arbacia punctulata* (figure 1.1), a species of sea urchin commonly found along the east coast of the United States and in the Gulf of Mexico [27]. Unlike mammalian reproduction, for which fertilization occurs internally, marine animals release their gametes into the ocean. For successful fertilization to occur in the vast marine environment, a complex dialogue must occur between gametes.

It is still not fully understood how this process occurs. How does the sperm know where the egg is? What is known is that it occurs via a process called chemotaxis (see Sec. 2.3). In summary, the urchin sperm move in the direction of an increasing concentration gradient of a specific protein released by the urchin egg. Experiments conducted by biologists such as Kaupp [21] [2] and Darszon [8] show that interaction with the protein signals an influx of calcium ions into the sperm. They also show that this influx of calcium is responsible for the change in sperm movement in the direction of the egg. Mathematicians and biologists such as Olson [25], and Jülicher et al [18] have successfully modeled sperm trajectory dependence on sperm calcium concentration and resact concentration, respectively. However they assumed reasonable, though artificially defined, calcium influxes to arrive at their results. It would be useful to have a model the accurately describes the natural influx of calcium into the sperm. This was not possible, however, because a model for the signaling process that occurs

between the egg protein and calcium influx had not yet been developed. Models have been developed for similar signal tranductions, though in other animals and cell types. These include models by Aoyama et al for goldfish retinal cells [3], and by Elad et al for rat uterine muscle cells [9]. The goal of this project is to model the chemotactic signaling process that results in calcium influx into the sea urchin sperm. With this knowledge, applications such as chemotactic drug delivery are made possible.

Chapter 2

Biological Background

2.1 Sperm

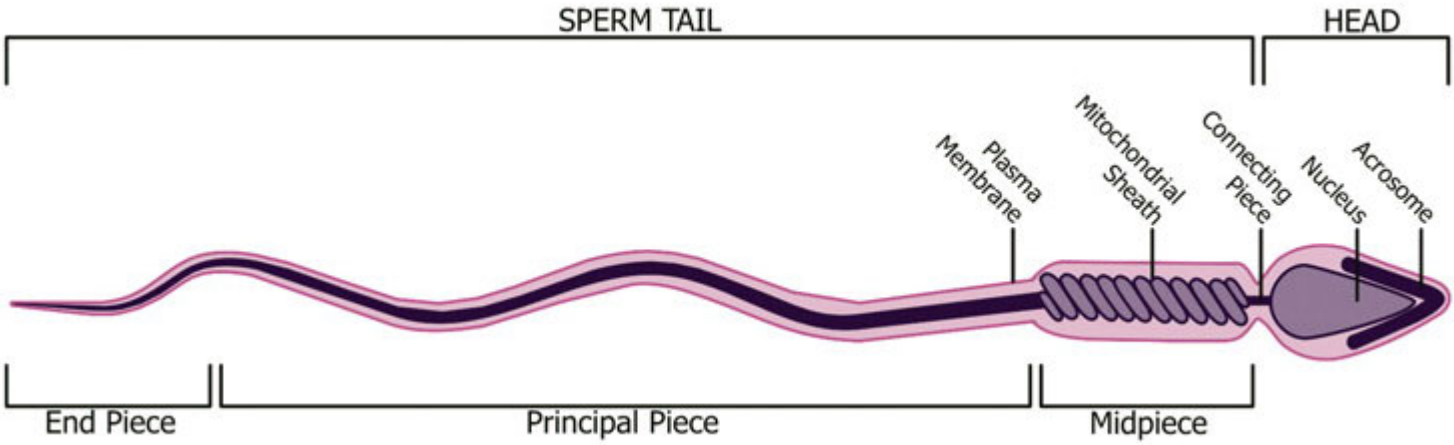

Figure 2.1: Diagram of sperm anatomy (reprinted from [10]).

Animal sperm generally have the layout shown in Fig. 2.1 in that they consist of a head (about 5 μm in length) and a tail or flagellum (up to 50 μm for invertebrates). The flagellum is further subdivided into the end piece and principal piece, which both oscillate to propel to the sperm, and the midpiece, which is densely populated with mitochondria that store the chemical energy used to oscillate the flagellum. Movement is important to sperm, since they are responsible for delivering genetic material to an egg and completing the fertilization process. In marine animals, they move primarily by chemotaxis towards the eggs (see Sec. 2.3) [21]. To do this, they rely heavily on their flagellum, which acts both as the propulsive machinery to move the sperm (see Sec. 2.4), as well as an antenna that detects chemical signals which guide their movement to the egg (see Sec. 2.4.1).

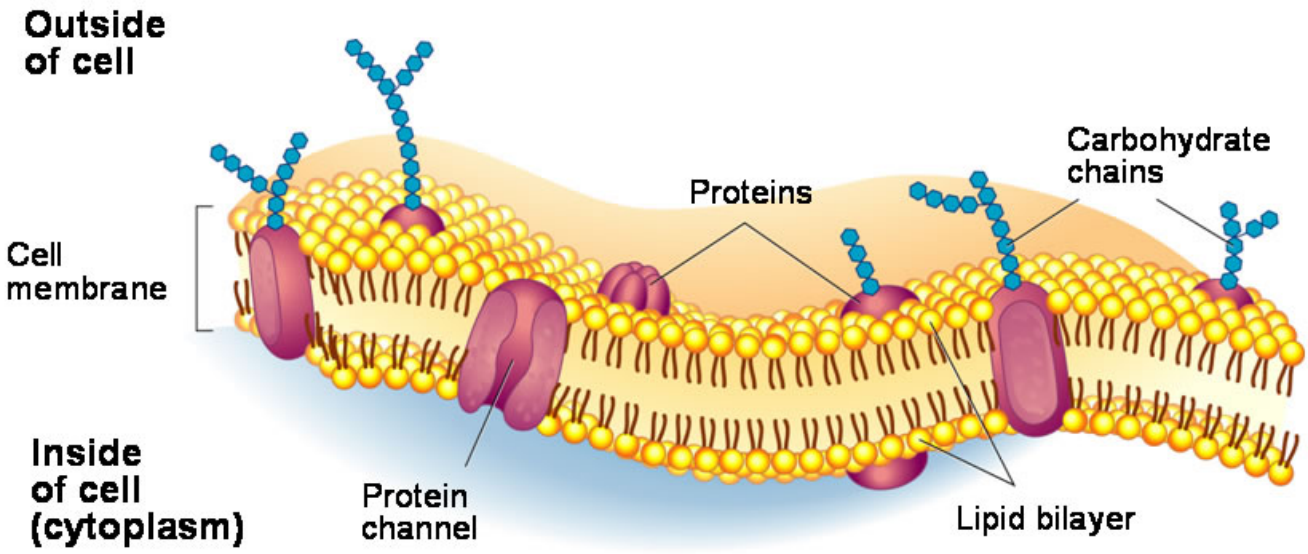

Figure 2.2: Typical elements of a cell membrane: a lipid bilayer with scattered protein channels and carbohydrate chains (reprinted from [13]).

2.2 Cell Membrane Potential and Ion Channels

2.2.1 Cell Membrane

All cells are enclosed in a cell membrane (or plasma membrane) that consists of a lipid (water-insoluble) bilayer embedded with proteins. Primarily, the membrane separates the interior of the cell from its environment. However, it is selectively permeable–permitting the free passage of some materials while restricting that of others–and thus also regulates material flow into and out of the cell [4].

The membrane facilitates material flow via various passive (no energy consumed) mechanisms [24]:

- Osmosis: movement of water up a chemical concentration gradient through small pores in the membrane.
- Simple diffusion: movement of chemicals down their concentration gradient through the pores in the membrane and, in the case of fat-soluble chemicals, through the membrane bilayer itself.
- Carrier-mediated diffusion: transport of chemicals across the membrane by proteins on the membrane. Chemicals either pass through pores in the transmembrane proteins, or bind to peripheral proteins which are then free to move to the opposing side of the membrane.

In addition, the membrane contains porous proteins called channels, which allow passage of specific molecules [24]. Channels actively transport chemicals against their concentration gradient, either by using cellular energy to "push" them (primary active transport), or using an energy inherent in an electrochemical gradient (secondary active transport). These active processes are important in cases where a cell might need to gather as much of a certain chemical as it can, for example glucose uptake by human intestinal cells. In reverse, cells may need to expel as much of a chemical as it can, for example Ca^{2+} ions, which become toxic at internal concentrations higher than 2 μM (typical external

concentration is 2000 μM in marine environments) [21]. Thus, sea urchin sperm are enclosed in a membrane that regulate the flow of materials into the cell. This will be important to the guidance of sperm toward the egg, though to understand why, we need to understand membrane potential.

2.2.2 Membrane Potential

The internal and external environments of cells consist of an aqueous solution of salts, primarily NaCl and KCl, which dissociate into Na^+, K^+, and Cl^- ions, especially in marine environments such as that of *A. punctulata*. The cell membrane prevents the free flow of these ions, though it does contain ion channels that allow specific ions to travel through the channels by active processes. Ion channels are channels that regulate cell volume by controlling the flow of specific ions across the membrane, and thus controlling the osmotic pressure in the cell [28].

Concentration differences are set up and maintained by active mechanisms that use energy to pump ions against their concentration gradient (Fig. 2.3). For example, Na^+ and K^+, found in all cells, work to keep internal K^+ concentrations high, while maintaining low internal Na^+ and Cl^- concentrations. Differences in ionic concentrations create a disparity in the charges on the interior and the exterior of the membrane, resulting in a potential difference across the cell membrane [28].

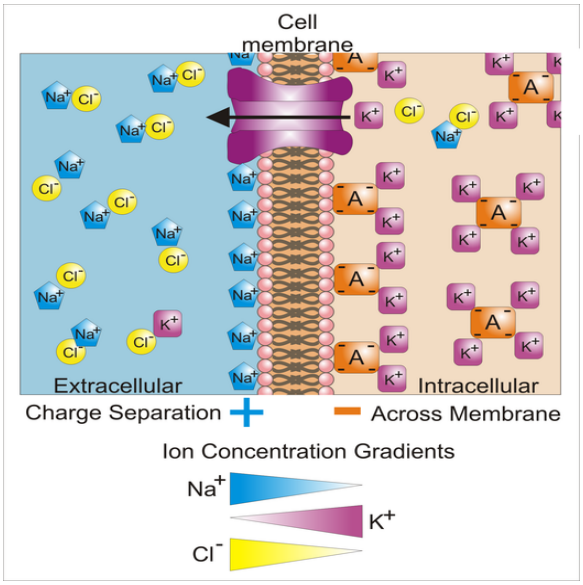

Figure 2.3: Ion channels work to keep different internal and external ionic concentrations. The disparity in ionic charges creates a potential difference across the membrane (reprinted from [30]).

The potential difference across the membrane when a cell is at rest, the resting potential, is usually negative. The resting potential of cells range from -10mV– -80mV [15].

Nernst Potential

Important to our model is the concept of Nernst potential, or reversal potential. The Nernst potential of an ion is the membrane potential that at which there is no net flow of that ion across the ion channel. We've mentioned previously that there are two forces governing ion flux across channels: diffusion due to concentration difference, and due to electric field difference. The concentration difference of an ion across the membrane results in a flow of that ion from one side to the other. However,

assuming other ion concentrations remain the same, the diffusion of an ion causes an imbalance of charge across the membrane which creates an electric field that opposes the further diffusion of that through the channel. Equilibrium of these two forces prevent ion movement across the membrane, and the membrane potential difference corresponding with this equilibrium is called the Nernst potential of ion in question. For the interested reader, a more detailed discussion of Nernst potential can be found in the work of James Sneyd [28].

Cell Signaling

The electrical activity of the cell can be used to communicate signals [21]. Changes in the membrane potential can trigger cell activities. Some ion channels may be opened by certain stimuli, such as binding with certain molecules or in response to previous changes to membrane voltage. For example, cyclic nucleotide-gated channels are channels, typically found in sperm cells, that are opened when a chemical called a cyclic nucleotide (such as cGMP) binds to the channel [21].

The opening of a channel results in a flow of ions that changes the membrane potential. Membrane depolarization occurs when the potential becomes more positive (or less negative). Depolarization is often caused by influx of positively charged ions (cations) such as Na^+ or Ca^{2+} through their respective channels. On the other hand, efflux of cations such as K^+, or the influx of anions such as Cl^- result in the membrane potential becoming more negative. This is called hyperpolarization.

These electrical mechanics are vital to communication in some cell species. In neurons, for example, a large enough depolarization may result in an "action potential" (Fig. 2.4) which form the basis of neuronal communication. Action potentials also lead to contractions in muscle cells and insulin release from pancreatic cells. Extensive work has been done on the causes and effects of action potentials, for example the work of Hodgkin and Huxley with giant squid nerve cells [16]. We will draw inspiration to achieve our goal to model sperm guidance toward the egg. Though, to do this, we will need to understand chemotaxis.

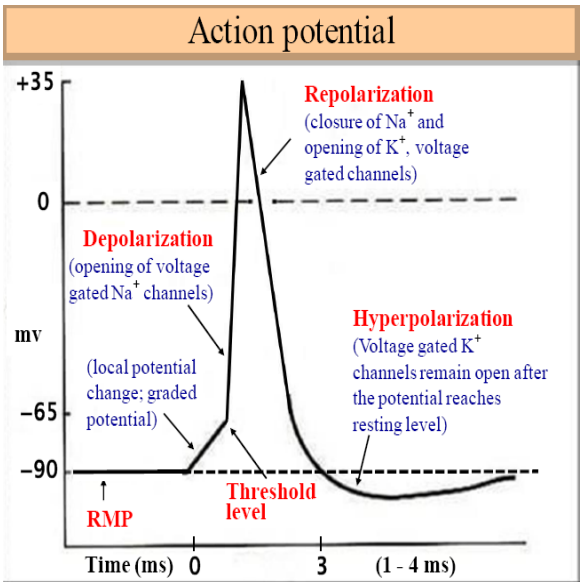

Figure 2.4: A schematic action potential (reprinted from [17])

2.3 Chemotaxis

Chemotaxis is the biased movement of an organism based on chemical concentrations in their environment. They have receptors sensitive to particular chemicals of interest so they can navigate their environment, relying on chemical signals to decide how, when, and where to move.

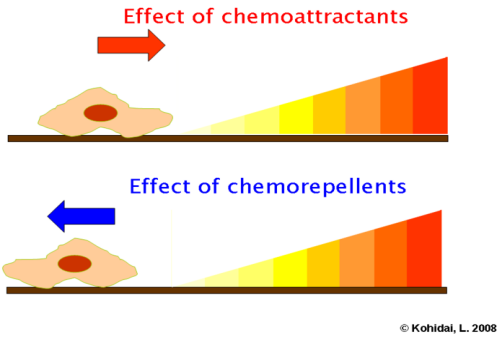

Figure 2.5: Chemotaxis: movement up (attractant) or down (repellent) a concentration gradient(reprinted from [22]).

A chemical is called a chemoattractant if a positive gradient attracts the organism–that is, it prefers to move closer to the source–and a chemorepellent if a positive gradient repels the organism, and so it prefers to move away from the source (Fig. 2.5). (Movement can be thought of mathematically as a biased random walk.)

Unicellular organisms such as bacteria locate and consume food primarily through chemotaxis, swimming (or more accurately, "running and tumbling") towards the highest concentration of food molecules. Even in multicellular organisms, individual cells such as the neutrophils deployed by the human immune system locate the site of an infection and track down infectious organisms to eat them via chemotaxis. During fetal development, chemotaxis also plays a role in the movement of cells as the organism develops; budding nerve cells, for example, start to distribute themselves to map out the nervous system. For a more detailed discussion of chemtotaxis, we refer the reader to work of Julius Adler [1].

Sexual reproduction for marine animals, for which fertilization occurs externally, also relies on chemotaxis. Sperm cells navigate the ocean waters to find the egg, following chemoattractants produced by the egg.

2.4 Mechanism of *A. punctulata* Sperm Chemotactic Signaling

The sperm of marine animals experience chemotaxis in similar ways, but the most extensive research on these mechanisms have been done on *Arbacia punctulata* sperm [21]. The eggs of *A. punctulata* are surrounded by a jelly coat that contains a protein called resact. The resact diffuses from the jelly coat into the ocean and forms a concentration gradient (lower concentrations farther from the egg) that cues the egg's location. Sperm detect that concentration gradient and adjust their swimming pattern to travel up that gradient (and so resact is a chemoattractant)(Fig. 2.6). When resact molecules (white area in Fig. 2.6a) bind to receptors on the sperm flagellum, it activates a signal pathway that excites the flagellum, which propels the sperm in the direction of the egg.

The ensuing Ca^{2+} dynamics stimulates an asymmetrical flagellar beat and adjusts the trajectory of the sperm. Stimulated sperm exit circular swimming pattern with tight loops (turns) and wide arcs (runs) up the resact gradient. This is depicted schematically in Fig. 2.6b.

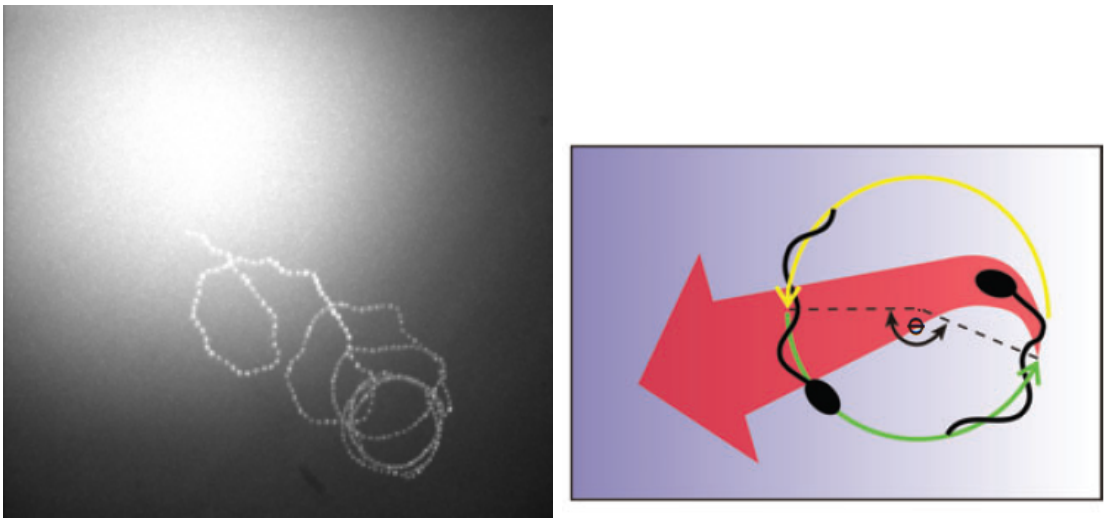

(a) **(b)**

Figure 2.6: 2.6a: Chemotaxis, as seen in experiments. The white area represents the source of resact (chemoattractant). Sperm swim in circles until they experience a surge in Ca^{2+} concentration, after which they make a sharp turn [21]; 2.6b: A schematic representation of the trajectory changes.

Experimental data shows the relationship between calcium flow into the sperm and trajectory [2]. In Fig. 2.7, we see the relationship between calcium concentration, measured by the fluorescence of a special dye, and the curvature of the sperm trajectory. After exposure to resact at 0 seconds, each peak in fluorescence corresponds with stimulation by resact, and occurs simultaneously with a sharp increase in path curvature. The increase in path curvature represents the sperm correcting its direction of movement toward the egg.

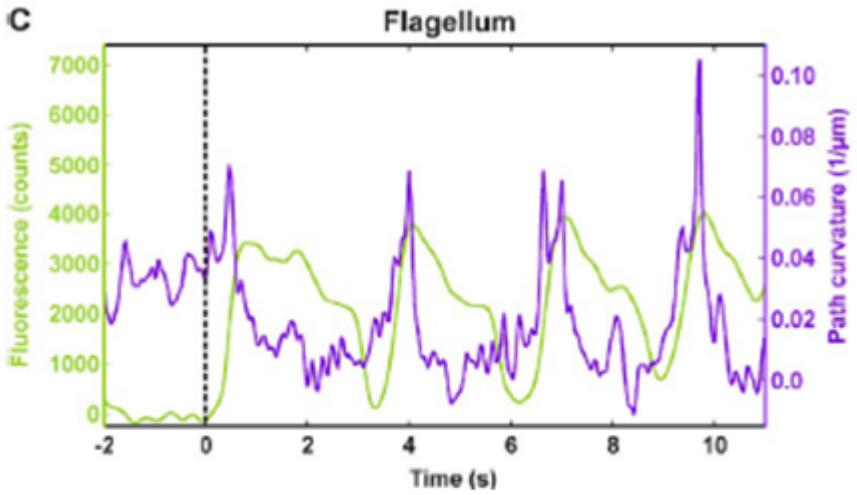

Figure 2.7: Changes in calcium concentration (represented as flourescence) during the chemotaxis cascade. Compared with swimming path curvature of the sperm [2].

2.4.1 Details of Signaling Pathway

Overview

The signaling pathway can be seen in Fig. 2.8. The membrane of the sperm flagellum contains a dense collection of receptor proteins called guanylyl cyclase (GC), with between about 10^4 and 10^6 receptors per flagellum [21]. Resact molecules, diffusing from the egg, bind to GC receptors on the flagellum tail membrane. The receptors can be sensitive to a single molecule. This causes the GC to synthesize a chemical called cyclic guanosine monophosphate (cGMP) which stimulates the opening of K^+-selective cyclic nucleotide-gated (KCNG) channels, which allow potassium ions into the sperm and induces membrane hyperpolarization (Fig. 2.8b). Hyperpolarization activates (but does not yet open) voltage-operated Ca^{2+} channels (VOCC), and also stimulates production of cyclic adenosine monophosphate (cAMP). cAMP opens hyperpolarization-activated cyclic nucleotide-gated (HCN) channels, which allow Na^+ out of the cell resulting in membrane depolarization. This depolarization opens the VOCC channels, which let Ca^{2+} ions into the cell.

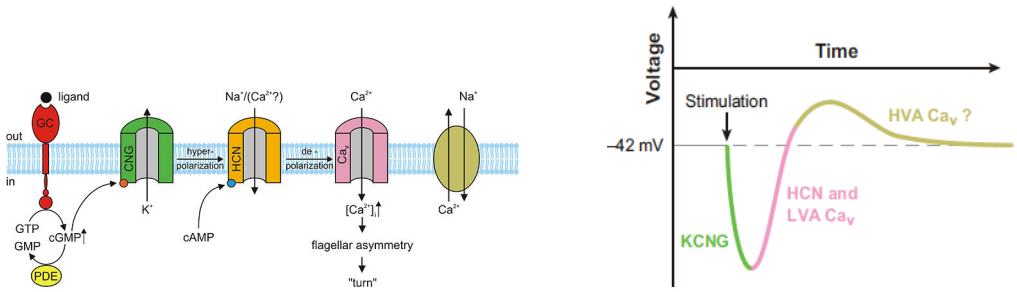

Figure 2.8: 2.8a: Channels on sperm membrane; 2.8b: Diagram of Membrane voltage during chemotaxis cascade (both reprinted from [21]).

KCNG channel

The K^+-selective cyclic-nucleotide-gated channel, or KCNG channel (the green channel in Fig. 2.8a), is the first channel in the signal pathway. It is a CNG ion channel (see Section 2.2.2) with a preference for K^+ ions. It opens upon stimulation by cGMP molecules, letting a K^+ current out of the cell. This induces membrane hyperpolarization, as depicted by the green segment of the voltage curve in Fig. 2.8b. Hyperpolarization activates, but does not yet open, the voltage-operated calcium channels [21].

The channel is composed of four homologous components. Each repeat contains a pore between and a binding domain for cyclic nucleotide phosphates. Hence, KCNG channels have four binding domains for cGMP. The channel has been shown to be also K^+-selective, that is, it allows only K^+ ions through. For a more detailed description of this channel, we refer the reader to the work of Darszon [8], Cukkemane [7], and Craven [6].

HCN channel

The hyperpolarization-activated cyclic-nucleotide-gated channels, or HCN channels (the orange channel in Fig. 2.8a) form the second stage of the pathway and are similar in structure to KCNG channels [8]. It opens in response to stimulation by cAMP molecules, as well as the hyperpolarization

induced by the KCNG. When open, it lets a Na^+ current into the cell, which induces membrane depolarization, as depicted by the pink segment of the voltage curve in Fig. 2.8b. As a results of this depolarization, the activated calcium channels open [21][8]. HCN channels open and close on a fast time scale naturally, and so have a small positive open probability. However, cAMP binding prolongs opening (and thus increases open probability), which promotes depolarization and calcium entry [7].

VOCC Channels

Voltage-operated Ca^{2+} channels, or VOCC channels (the pink channel in Fig. 2.8a), activate when the membrane is hyperpolarized by the KCNG, and then open when depolarized by the HCN [21]. VOCC channels allow a Ca^{2+} current into the cell, and so are key to chemotactic signaling. Again, they are similar in structure to the KCNG. Voltage sensors on the channel detect voltage and changes the conformation of the channel pore. This channel closes in response to elevated calcium concentrations, causing the sperm cell to adapt to high concentrations of calcium. It recovers from inactivation when membrane is hyperpolarized by KCNG, leading to a periodic process. Since the hyperpolarization spreads passively accross the membrane, all VOCCs along the flagellum membrane are affected and recover from inactivation and eventually open. [21].

PMCA Channel

The plasma membrane Ca^{2+} ATPase (PMCA) channel is not specific to the chemotactic calcium signaling chain, but passively affects intracellular calcium concentration and is still key to sperm chemotactic signaling and motility [14]. PMCA channels are transmembrane channels with high affinity for calcium ions. They selectively pump free calcium ions out of the cell via primary active tranport to maintain low internal Ca^{2+} concentrations ($< 1\ \mu$M). This action is important because consistently high concentrations of intracellular Ca^{2+} have been shown to inhibit sperm motility and even trigger cell death [14].

Na^+-Ca^{2+} Exchanger (NCX) Channel

Like PMCA, this channel is not specific to the chemotactic calcium signaling chain, but works in the background to keep intracellular Ca^{2+} concentrations low. NCX channels are transmembrane channels that work via secondary active tranport, using the energy inherent in electrochemical gradient to push Ca^{2+} ions out of the cell in exchange for the entry of Na^+ ions (with a ratio of $3Na^+ : 1Ca^{2+}$). Also like PMCA, they have been shown to be necessary for sperm motility, and so are also key to sperm chemotactic signaling [29].

Chapter 3

Modeling Background

3.1 Hodgkin-Huxley Models

We have seen in Chapter 2 that cell channel mechanisms result in a membrane potential difference, which controls ion flow through the membrane channels. To understand these processes, Hodgkin and Huxley created models to describe the cell membrane voltage during their 1952 study of neuron action potentials. The models are derived by considering the circuit analog to the components of the cell (Fig. 3.1).

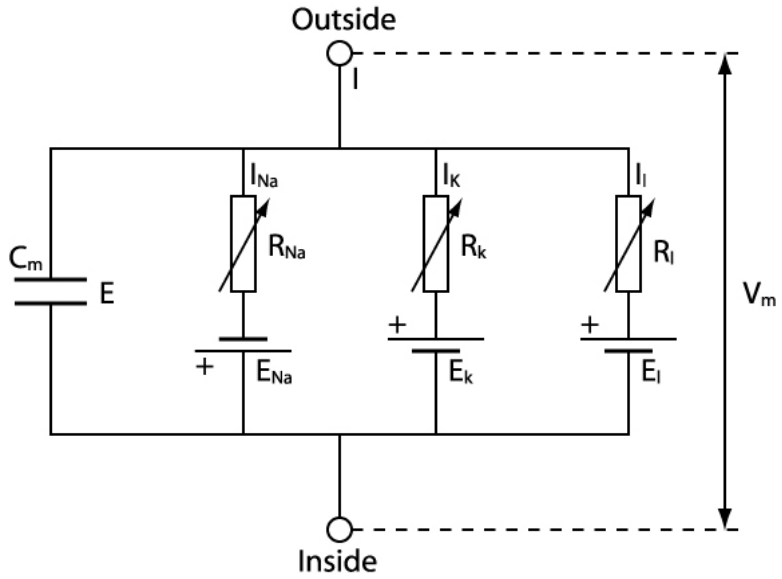

Figure 3.1: Circuit analogy of the cell membrane: Hodgkin and Huxley likened the cell membrane to a circuit, with a capacitance (lipid bilayer) in parallel with variable resistors (ion channels) of a specific conductance, which are in turn in series with a power supply (reversal potential)(reprinted from [8]).

The lipid bilayer separates charges (Fig. 2.3) and so can be thought of as a capacitor. Capacitance is defined as the ratio of the charge across the capacitor to the voltage potential necessary to hold that charge. Thus, we can describe the membrane capacitance, C_m, by

$$C_m = \frac{Q}{V_m} \ , \tag{3.1}$$

where Q represents charge, and V_m is the membrane voltage.

Taking the outward direction to be positive, current I is defined by $I = \frac{dQ}{dt}$. Hence, we can see that the current through the capacitor, I_C, is given by

$$I_C = C_m \frac{dV_m}{dt} \ . \tag{3.2}$$

The capacitor (lipid bilayer) is connected to parallel resistors, each resistor representing an ion channel. By Kirchhoff's Current Law, the sum of the ionic and capacitive currents must be zero. That is, if we consider the current I_i, where the subscript i denotes the i–th specific ion channel, then we have

$$I_C + \sum_i I_i = C_m \frac{dV_m}{dt} + \sum_i I_i = 0 \ . \tag{3.3}$$

Determining an appropriate expression for I_i can be challenging. Note that the resistors (channels) are in series with power supplies, which represent the Nernst potential, E_i, of the corresponding ion i (see Sec. 2.2.2). Hodgkin and Huxley proposed that the current I_i was related to the difference in membrane voltage and Nernst potential in the following way. Consider the movement of an ion i across a membrane. The change in membrane potential caused by this ion flow is affected in two ways. The first is due to the to concentration differences (and thus, charge imbalance). The effect of this is governed by the Nernst potential of i, which is given by the Nernst equation

$$E_i = \frac{RT}{zF} \ln \frac{[i]_{ex}}{[i]_{in}} \ , \tag{3.4}$$

where R is the universal gas constant, F is Faraday's constant, and z is the valence of ion i (for parameter values, see Appendix B). Here, the subscript ex denotes the external ionic concentration, and in denotes the internal concentration. The second is due to the electrical current. By assuming the channels are ohmic, the potential drop due to an electrical current is $r_i I_i$, where r_i is the channel resistance. Summing these two contributions, we find the change in membrane potential due to ion flux is given by

$$V = r_i I_i + E_i \ , \tag{3.5}$$

and solving for the current, we get the current–voltage relationship

$$I_i = g_i (V - E_i) \ , \ g_i = \frac{1}{r_i} \ . \tag{3.6}$$

Here, we use the channel conductance, or reciprocal resistance, g_i, for a clearer intuition of channel behavior. In reality, the resistors are not necessarily ohmic, as the conductance of the channels are voltage dependent.

Thus, the change in potential across the membrane with respect to time is proportional to the sum of the currents across the membrane ion channels, and is given by

$$C_m \frac{\mathrm{d}V_m}{\mathrm{d}t} = -\left(\sum_i I_i \right) \ , \tag{3.7a}$$

$$I_i(V_m, t) = g_i (V_m - E_i) \ . \tag{3.7b}$$

3.2 Parameter Estimation

Parameter estimation encompasses the techniques used in mathematical modeling of phenomena and the estimation of constants appearing in these models. It is useful because:

- Many of the parameters gathered from research papers are given in a range and/or vary between sources.
- Some of our parameters are not "sea urchin sperm specific", that is, they were taken from models of similar phenomena in different cells of other animals, such as rat uterine muscle and goldfish retinal cells. The values of these parameters may be similar to their urchin sperm specific counterparts in some cases, but may differ greatly in others.

The model ODEs are difficult to solve analytically, and so we estimate the parameters directly from the ODEs. That is, we solve the ODEs on each iteration of the estimation process.

3.2.1 Algorithm

Let $\mathbf{p}$ be the m-dimensional vector of parameters to be estimated, where m is the number of parameters to be estimated. We can write an n-dimensional ODE system described by

$$\mathbf{y}' = f(t, \mathbf{y}; \mathbf{p}) \ , \ \mathbf{y} \in \mathbb{R}^n \ . \tag{3.8}$$

Let $\mathbf{z}$ be the vector which is the observed output of the system to be modeled, that is, the vector of expected results. We can optimize the parameters $\mathbf{p}$ by minimizing the following:

$$\mathcal{F} = \sum_k \left(f(t_k, \mathbf{y}; \mathbf{p}) - z_k\right)^2 \ , \tag{3.9}$$

where the sum is taken over the k data points. Our cost function $\mathcal{F}$ is a least squares (Euclidean norm), which is useful because we want to minimize the distance between the points of our numerical solution and those of the expected solution $\mathbf{z}$. In this way, it is not necessary for our solution attain each expected value, but that it comes as close as it can to all expected values.

The algorithm to estimate parameters is as follows:

1. Solve the n-dimensional ODE system numerically, using an initial parameter vector $\hat{\mathbf{p}}$.
2. Evaluate cost function $\mathcal{F}$.
3. Iterate the Nelder-Mead optimization routine to update $\hat{\mathbf{p}}$ (see Sec. 3.2.2).
4. Evaluate $\mathcal{F}$ with updated $\hat{\mathbf{p}}$ and compare with previous objective value.
5. Repeat (1.)–(4.) until the mininum of $\mathcal{F}$ is obtained, or the result of (3.) is stable. Name this vector $\mathbf{p}$.

The resulting vector $\mathbf{p}$ is the optimal parameter vector for the ODE.

3.2.2 Nelder-Mead

The Nelder–Mead optimization routine is a commonly used nonlinear optimization routine developed by John Nelder and Roger Mead in 1965. The method approximates a local minimum of a cost function problem with m variables—each variable representing a parameter—by constructing the simplex determined by those points. A simplex is polytope of $m+1$ vertices in an m–dimensional space [26]. More formally, A simplex in $\mathbb{R}^m$ is a set of $m+1$ points $\mathbf{x_0}, \ldots, \mathbf{x_m} \in \mathbb{R}^m$ such that the set of vectors $\{\mathbf{x_i} - \mathbf{x_0} : i = 1, \ldots, m\}$ is linearly independent in $\mathbb{R}^n$.

The Nelder–Mead algorithm generates a simplex of test points in parameter space. It then extrapolates the behavior of the objective function measured at each test point along a line through that point and the centroid of the simplex, and then determines the worst test point (the point with the highest objective value). The algorithm then modifies the simplex by way of reflection, contraction, expansion, and/or shrinking about the centroid to replace the worst test point with a better one. This continues until the simplex is "very flat", that is, the function value is almost the same at all the vertices. The minimum of the function is taken to be the vertex with the smallest function value. For more information on then Nelder–Mead method, we invite the reader to the work of Powell [26].

3.3 Polynomial Interpolation

Biologists perform experiments that produce data. The data are typically in the form of data points, each point representing the value of a quantity at a specific, discrete time point. Oftentimes we are interested in the values of that quantity at intermediate time points not measured by the experiment. Interpolation is a method of estimating those values of the dependent variable at intermediate time points. One method of interpolation involves fitting a polynomial to the data points.

Formally, given n data points $(x_i, y_i), i = 1, \ldots n$, an interpolating polynomial $p(x)$ is a polynomial of degree at most $n-1$ such that $p(x_i) = y_i$.

For a large number number of data points, high-degree polynomials tend to oscillate, leading to unrealistic and inaccurate estimations. This can be solved using a related technique call spline interpolation. With spline interpolation, low-degree polynomials are used to interpolate each interval. Hence, the result is a piecewise function of $n-1$ polynomials, each chosen so that they fit smoothly together. Spline interpolation is preferred over polynomial interpolation because the interpolation error can be made small even when using low degree polynomials for the spline.

The polynomials were found using MATLAB functions pchip.

Chapter 4

Modeling the Signal

In this chapter, we will develop model equations to track the time derivative of membrane voltage, as well as the calcium flux into the cell. We are simplifying the geometry of the sperm tail and using a whole–cell model. That is, we will assume a uniform density of membrane channels along the sperm tail membrane, and consider uniform distribution of charged ions both inside and outside the cell. This will allow us to define the membrane potential as the difference between the average electrical potential inside and the average potential outside. We also take the the calcium influx to be the total amount of Ca^{2+} ions across the cell. This approach is supported by the work of Kaupp [21], in which it is discovered that changes in membrane voltage at one point on the membrane passively and immediately spreads throught the entire sperm tail.

4.1 Membrane Potential

Calcium is let into the cell by voltage-dependent channels (VOCCs, see Sec. 2.4.1), and so to model calcium flux, we need a model for membrane voltage. To do this, we use equation (3.7a) to say that the membrane voltage of the whole cell is governed by

$$C_m \frac{dV_m}{dt} = -(I_{KCNG} + I_{HCN} + I_{VOCC} + I_{leak} + I_{PMCA} + I_{NCX}) \ . \tag{4.1}$$

- V_m represents the membrane potential in mV, C_m represents the membrane capacitance in pF.
- I_i represents the current in pA through the relevant signaling ion channels (see Sec. 2.4.1).
- In the differential equation, the standard practice is to give each current the same sign (as seen in [3] [19] [31] [23]). The sign (direction) of each current is determined by the reversal potential—specifically the difference between the instantaneous membrane potential and the channel's reversal potential. We take outward current to be positive.
- By tracking the values of V_m and I_{VOCC}, we can determine the Ca^{2+} flux across the sperm membrane (see Sec. 4.3).

4.2 Channel Models

4.2.1 KCNG Channel

The KCNG channel lets a K^+ current out of the cell to induce membrane hyperpolarization, which activates (but does not open) VOCC channels [21]. Using the Hodgkin-Huxley model (3.7b), we can represent the current flow through the KCNG channel by

$$I_{KCNG} = g_{KCNG}(V_m - E_{KCNG})\ [pA], \tag{4.2}$$

where E_{KCNG} represents the reversal potential of K^+ in mV, and g_{KCNG} represents the conductance of KCNG channel in nS. The KCNG channel is not ohmic. In fact, the conductance of the channel is non-linearly related to voltage by

$$g_{KCNG} = \bar{g}_{KCNG} n^4\ [nS]. \tag{4.3}$$

Thus, we have

$$I_{KCNG} = \bar{g}_{KCNG} n^4 (V_m - E_{KCNG})\ . \tag{4.4}$$

Here, $\bar{g}_{KCNG}$ represents the maximum conductance of the KCNG channel (a constant). The n term is called the gating activation variable for the channel, which represents the proportion of the total number of channels on the membrane that are open. Hence, n is dimensionless and ranges from 0–1, and the greater n is, the more current passes through the channel. The gating variable n satifies the differential equation

$$\frac{dn}{dt} = [n_\infty(V_m) - n]k_n(V_m)\ , \tag{4.5}$$

where $n_\infty(V)$ represents the steady state activation of the channel, and $k_n(V)$ represents the activation rate. Both terms are dependent on voltage, and are given by

$$n_\infty(V) = \frac{1}{\left(1 + \exp\left(\frac{V - V_n}{s_n}\right)\right)} \left(\frac{[cGMP]^H}{K_{cGMP}^H + [cGMP]^H}\right)\ , \tag{4.6}$$

$$k_n(V) = \frac{c_n}{\left(1 + \exp\left(\frac{V - V_{kn}}{s_{kn}}\right)\right)}\ [ms^{-1}]. \tag{4.7}$$

Here, V_n represents the half-maximal potential in mV, that is, the potential at which $n_\infty(V) = \frac{1}{2}$, and s_n represents the step width of the curve in mV, the range potentials centered at V_n over which $n_\infty(V)$ goes from ~ 0 to ~ 1. The terms V_{kn} and s_{kn} represent the same for $k_n(V)$, respectively. Note that the step widths can be either positive or negative: a negative step width indicates a function that increases with V (activation), while a positive step width indicates a function that decreases with V (inactivation). Also note the dependence of the steady state activation on cGMP concentration. This reflects the channels dependence on cGMP concentration [6] [8] (see Sec. 2.4.1). With the chosen term, the channel operates at "natural" steady state activation when cGMP concentration is zero. The steady state activation increases when cGMP is introduced, in proportion to the Hill expression with Hill coefficient H and dissocciation constant K_{cGMP}.

cGMP mechanics

The activity of the KCNG channel is stimulated in the presence of cGMP. cGMP is synthesized when resact binds to the membrane of the flagellum, and so the interal concentration of cGMP is coupled with the external concentration of resact. However, biologists conducting experiments on sperm chemotactic behavior typically use a photocage release of a fixed amount of cGMP into the cells, skipping that first step of resact interaction. Thus, there is little information from a modeling point of view on how resact influences cGMP synthesis. However, there is data relating changes in internal cGMP conentration with time when the sperm is exposed to certain levels of resact. We can use this data in two ways:

- We can develop an interpolating polynomial that accurately represents the cGMP concentration data with respect to time (see Chap. 5).
- We propose the relationship between cGMP and resact concentrations with respect to time can be given by

$$\frac{d[cGMP]}{dt} = q_1[R] - q_2\frac{[cGMP]^2}{[cGMP]+q_3}\ [\mu M m s^{-1}], \tag{4.8a}$$

$$\frac{d[R]}{dt} = -q_4[R]\ [\mu M m s^{-1}]. \tag{4.8b}$$

Here, cGMP concentration increases in direct proportion to the resact concentration, with a rate of q_1 ($[ms^{-1}]$). It also decreases in proportion to the product of its current concentration and the Michaelis-Menten kinetics of enzyme degradation with Michaelis constant q_3 ($[\mu M]$), at a rate of q_2 ($[ms^{-1}]$) [19]. The resact concentration $[R]$ degrades exponentially with rate constant q_4 ($[ms^{-1}]$). We find values of parameters q_1, q_2, q_3, q_4 that give a "best fit ODE" to the experimental data using parameter estimation with Nelder-Mead optimization (see Chap. 5).

4.2.2 HCN Channel

The HCN channel opens in response to the hyperpolarization induced by the KCNG, as well as to stimulation by cAMP molecules. It lets a Na^+ current into the cell, which induces membrane depolarization. Using the Hodgkin-Huxley model (3.7b), we can represent the current flow through the HCN channel by

$$I_{HCN} = g_{HCN}(V_m - E_{HCN})\ [pA], \tag{4.9}$$

where E_{HCN} represents the reversal potential of Na^+ in mV, and g_{HCN} represents the conductance of HCN channel in nS. Like the KCNG channel, the HCN is not ohmic, with the conductance of the channel related to voltage by

$$g_{HCN} = \bar{g}_{HCN} r\ [nS]. \tag{4.10}$$

Thus, we have

$$I_{HCN} = \bar{g}_{HCN} r(V_m - E_{HCN})\ . \tag{4.11}$$

Here, $\bar{g}_{HCN}$ represents the maximum conductance of the KCNG channel in nS, and r is the dimensionless gating activation variable for the channel, which satifies the differential equation

$$\frac{dr}{dt} = [r_\infty(V_m) - r]k_r(V_m)\ , \tag{4.12}$$

where $r_\infty(V)$ represents the steady state activation of the channel, and $k_r(V)$ represents the activation rate. Both terms are dependent on voltage, and are given by

$$r_\infty = \frac{1}{\left(1 + \exp\left(\frac{V - V_{kr}}{s_{kr}}\right)\right)} \ , \tag{4.13}$$

$$k_r(V) = c_r \left(1 + \exp\left(\frac{V - V_{kr}}{s_{kr}}\right)\right) \ [ms^{-1}]. \tag{4.14}$$

Here, V_r represents the half-maximal potential of $r_\infty(V) = \frac{1}{2}$, and s_r represents the step width of the curve. The terms V_{kr} and s_{kr} represent the same for $k_r(V)$, respectively.

4.2.3 VOCC Channel

Voltage-operated Ca^{2+} channels (VOCC) activate when the membrane is hyperpolarized by the KCNG, and then open when depolarized by the HCN [21]. VOCC channels allow a Ca^{2+} current into the cell, and so are key to chemotactic signaling. Again, using the Hodgkin-Huxley model (3.7b), we can represent the current flow through the VOCC channel by

$$I_{VOCC} = g_{VOCC}(V_m - E_{VOCC}) \ [pA], \tag{4.15}$$

where E_{VOCC} represents the reversal potential of Ca^{2+} in mV, and g_{VOCC} represents the conductance of HCN channel in nS.

The Nernst potential for the VOCC channel is found using (3.4)

$$E_{VOCC} = \frac{RT}{2F} ln \left(\frac{[Ca^{2+}]_{ex}}{[Ca^{2+}]_{in}}\right) \tag{4.16}$$

Like the KCNG and HCN channels, the VOCC channel is not ohmic, with the conductance of the channel related to voltage by

$$g_{VOCC} = \bar{g}_{VOCC}\rho \ . \tag{4.17}$$

Thus, we have

$$I_{VOCC} = \bar{g}_{VOCC}\rho(V_m)(V_m - E_{VOCC}) \ . \tag{4.18}$$

Here, $\bar{g}_{VOCC}$ represents the maximum conductance of the VOCC channel in nS, and ρ is the dimensionless gating activation variable for the channel, which is given by

$$\rho(V) = \frac{1}{1 + \exp\left(\frac{V_\rho - V}{s_\rho}\right)} \ . \tag{4.19}$$

Here, V_ρ represents the half-maximal potential of $\rho(V) = \frac{1}{2}$, and s_ρ represents the step width of the curve.

4.2.4 Leakage

Though the cell membrane is impermeable to ions, the large difference between internal and external concentrations can overwhelm the membrane and results in some ions passing through. This is called leakage. We can localize the leakage, and assume it occurs through a "leakage channel" on the membrane. We can then use (3.7b) to represent current leakage by

$$I_{leak} = g_{leak}(V_m - E_{leak})\ [pA], \tag{4.20}$$

where E_{leak} represents the reversal potential of the leakage channel in mV, and g_{leak} represents the conductance of the leakage channel. For simplicity, we assume this channel is ohmic, and so g_{leak} is constant.

4.2.5 PMCA Channel

PMCA channels selectively pump free Ca^{2+} ions out of the cell via primary active tranport to maintain low internal Ca^{2+} concentrations. These channels are typically modeled using a Hill equation, rather than with Hodgkin-Huxley dynamics. We have

$$I_{PMCA} = i_{PMCA}\left(\frac{[Ca^{2+}]_{in}}{K_{PMCA} + [Ca^{2+}]_{in}}\right)\ [pA]. \tag{4.21}$$

Here, the Hill expression with a Hill coefficient of 1 and dissocciation constant K_{PMCA} ($[\mu M]$) represents Ca^{2+} movement due to active transport. To find the current through the PMCA, we multiply this expression by i_{PMCA}, the maximum current possible through the channel in pA [20].

4.2.6 NCX Pump

NCX pumps remove internal Ca^{2+} ions in exchange for the entry of Ca^{2+} ions. The standard model for the outward current of the NCX pump involves tracking internal sodium concentration, which is troublesome. A simpler equation due to Aoyama [3] [describing retinal NCX in goldfish] is given by

$$I_{NCX} = i_{NCX}\lambda\frac{[Ca^{2+}]_{in}}{[Ca^{2+}]_{in} + K_{NCX}}\ [pA], \tag{4.22}$$

Again, we have a Hill expression with a Hill coefficient of 1 and dissocciation constant K_{NCX} ($[\mu M]$) represents Ca^{2+} movement due to active transport. To find the current through the NCX, we multiply this expression by i_{NCX}, the maximum current possible through the channel in pA [20], as well as the gating variable λ given by

$$\lambda = \exp\left(\frac{V_m - V_\lambda}{s_\lambda}\right). \tag{4.23}$$

Here, V_λ represents the half-maximal potential of λ and s_λ represents the step width of the curve.

4.3 Calcium Concentration

The channels responsible for calcium flux are the VOCC, the NCX, and the PMCA. In general, we can determine the outward ion flux, J_{ion}, through a channel from the relationship

$$J_{ion} = \frac{I_{ion}}{\nu F v} 10^{-9} \ [\mu M m s^{-1}]. \tag{4.24}$$

Here, F is Faraday's constant, v is the volume of the sperm flagellum, and ν is the valence of calcium [9] [3]. We scale by 10^{-9} to make this quantity consistent with our units.

Thus, we can describe the net inward flux of Ca^{2+} ions by

$$\frac{d[Ca^{2+}]}{dt} = -(J_{VOCC} + J_{NCX} + J_{PMCA}) + J_{leak} \ . \tag{4.25}$$

Here, J_{leak} is a small constant that represents the small amount of Ca^{2+} leakage into the sperm cell. We subtract the flux J_{VOCC}, J_{NCX}, and J_{PMCA} because of the sign convention for current direction. The VOCC channel lets a Ca^{2+} current into the cell, and thus increases the internal calcium concentration of the cell. However, we take an outward to be positive, and so I_{VOCC}, and by extension J_{VOCC}, are negative. Similarly, the NCX pump and PMCA channel let a Ca^{2+} current out of the cell, and so J_{VOCC} and J_{NCX} are positive, but decrease internal calcium concentration.

Chapter 5

Results

5.1 cGMP Model

We have previously mentioned that there is little information, from a modeling perspective, on the relationship between resact concentration and the production and degradation of cGMP. However, biologists such as Kaupp and Darszon have measured the concentration of cGMP in response to various resact concentrations [8].

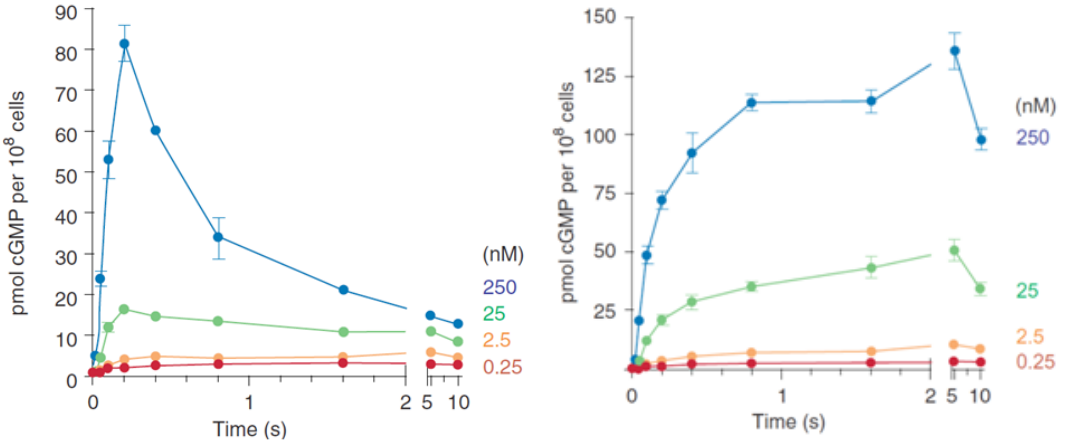

Figure 5.1: 5.1a: Measured cGMP concentration, in pmol per 10^8 cells, in *A. punctulata* sperm cells in response to various concentrations of resact.; 5.1b: Measured cGMP concentration in response to the same concentrations of resact, and the chemical IBMX, which blocks the degradation of cGMP (reprinted from [8])

.

From the graphs in Fig. 5.1, we can see how internal cGMP concentration changes over time when the sea urchin sperm is exposed to concentrations of resact ranging from 0.25nM to 250nM. In Fig. 5.1a, we see that cGMP concentrations rise quickly and peak at about 200 ms, after which there is degradation. Fig. 5.1b shows the cGMP concentration time course in the presence of a chemical called IBMX, which inhibits the degradation of cGMP. We see it rises to higher peak values at the same rate and then levels off.

We can use polynomial interpolation to estimate the change in cGMP concentration over time. To

interpolate the data, we use piecewise cubic Hermite interpolating polynomials from the MATLAB function `pchip`. However, the data was presented in pmol/10^8 cells. We converted this information to μM for a single cell by:

$$y = \frac{x \times 10^{-6}}{10^8 \times Volume} \tag{5.1}$$

where x is the raw data (pmol/10^8 cells) and y has our desired unit of μM for a single cell. The volume a sperm tail is $45\pi \times 10^{-15}$dm^3 (Table B.1).

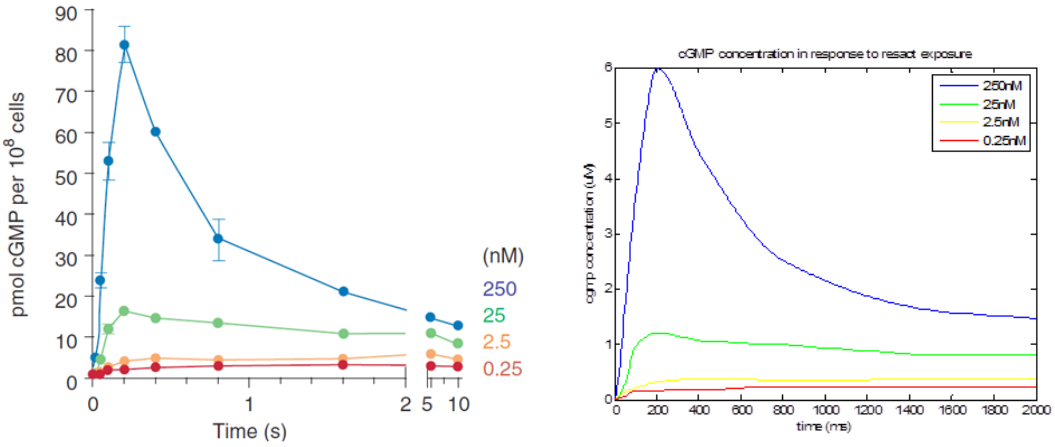

(a) **(b)**

Figure 5.2: Comparison between the cGMP time course data in Fig. 5.1a and the spline interpolation of that data, in μM.

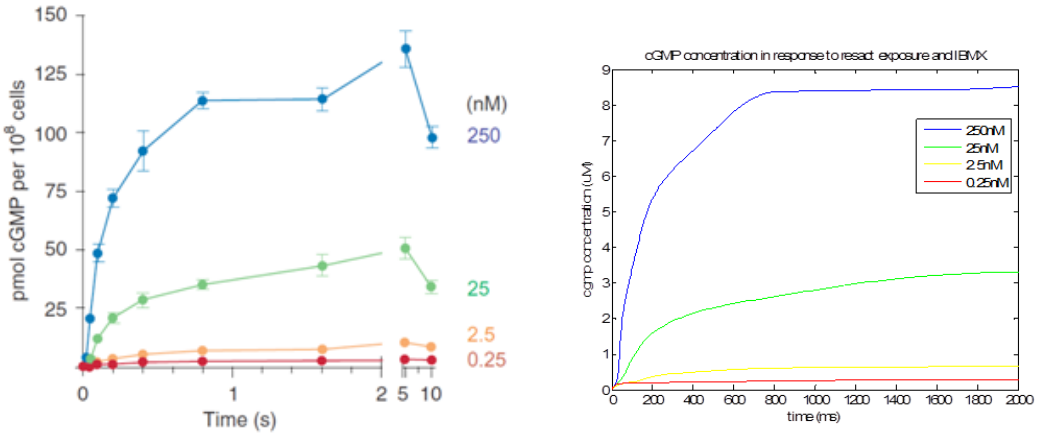

(a) **(b)**

Figure 5.3: Comparison between the cGMP time course data, in the presence of IBMX, in Fig. 5.1b and the spline interpolation of that data, in μM

.

The interpolants, as shown in Figs. 5.2b and 5.3b fit the general shape of the data shown in Figs. 5.2a and 5.3a, respectively. We can feed this polynomial interpolant into the full model equation for the KCNG channel's dependence on cGMP concentration (see eqn. (4.6)). However, we went a step further to describe this time course data with a system of differential equations.

In section 4.2.1, we proposed a relationship between cGMP and resact concentrations, inspired by the literature, with the following ODE:

$$\frac{d[cGMP]}{dt} = q_1[R] - q_2\frac{[cGMP]^2}{[cGMP]+q_3} \ , \tag{5.2a}$$

$$\frac{d[R]}{dt} = -q_4[R] \ , \tag{5.2b}$$

$$\tag{5.2c}$$

where cGMP concentration increases in proportion to resact concentration with rate constant q_1, and decreases according to Michaelis-Menten kinetics with rate constant q_2 and Michaelis constant q_3. The resact concentration $[R]$ degrades exponentially with rate constant q_4. We used parameter estimation techniques (Sec. 3.2) to find q_1, q_2, q_3, q_4 that give a "best fit ODE" to the interpolated data.

Steady State Analysis and Parameter Estimation

To start the parameter estimation process, we need an initial guess for q_1, q_2, q_3, and q_4. We can perform steady state analysis on the inerpolant by picking an appropriate point on the graph where the dervative is approximately zero, and identifying the ratio between the parameters at the point. One such point is on the graph of cGMP concentration at 250nM resact, $[cGMP] \approx 6\mu$M. The corresponding resact concentration is $[R] \approx 0.2\mu$M. Therefore we can say,

$$0 = q_1(0.2) - q_2\frac{(6)^2}{7}$$

and so

$$\frac{q_1}{q_2} = \frac{(6)^2}{(7\times 0.2)} \approx 25$$

Therefore we know q_1 is greater than q_2 by a factor of 25 (or by 1 order of magnitude). With this, we arrive at more accurate guesses for initial parameter values. We then try to find parameters using the Nelder-Mead routine (see Sec. 3.2.2) that minimize the cost function

$$\mathcal{F} = \sum \left(P(t) - [cGMP](t;\mathbf{q})\right)^2 \ ,$$

where $P(t)$ is the interpolating polynomial for cGMP concentration with time and $[cGMP](t;\mathbf{q})$ is the solution to equation (5.2a) with parameter vector $\mathbf{q} = (q_1, q_2, q_3, q_4)$. Note that we numerically solve the ODE using MATLAB function `ode45` on each iteration of the Nelder-Mead routine. The code for this process can be found in Appendix C.2.2. A visualization of the process can be seen in Fig. 5.4. The Nelder-Mead method searches the 4–dimensional parameter space for values that minimize $\mathcal{F}$. With each iteration, a new test point is generated and the least squares error of the numerical solution of the ODE is compared to the error of the previous iterate. Fig. 5.4 shows how the parameters and the error change with each iteration.

Minimizing this function, we get parameter values $q_1 = 0.0147$, $q_2 = 0.7432$, $q_3 = 1693.2422$, $q_4 = 0.0012$, after 567 iterations and with an error of $\mathcal{F} = 3.4\times 10^{-4}$. A comparison between the data and the solution of the ODE can be seen in Fig. 5.5.

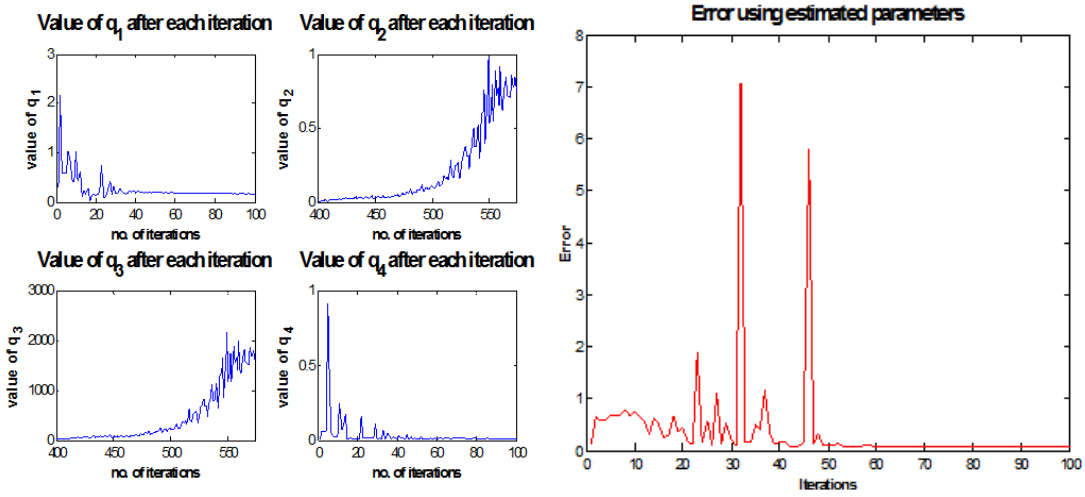

(a) (b)

Figure 5.4: Visualization of parameter estimation process. Figure 5.4a shows the test values of the parameters q_i after each iteration of Nelder-Mead optimization. Figure 5.4b shows the change in error with each iteration.

.

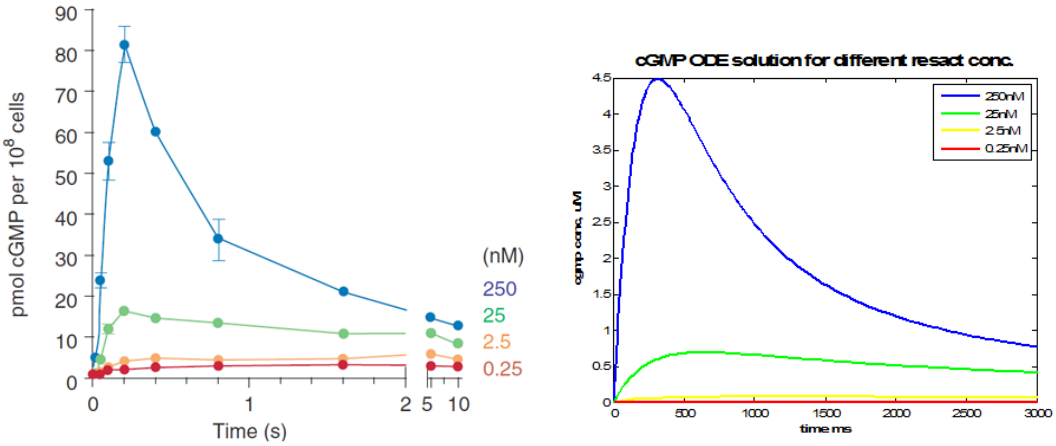

(a) (b)

Figure 5.5: Comparison between interpolated data and ODE solution with $q_1 = 0.0147$, $q_2 = 0.7432$, $q_3 = 1693.2422$, $q_4 = 0.0012$

.

5.2 Full Model

We went on to apply parameter estimation techniques to the whole model. By combining the six equations (4.1),(4.5),(4.8) (a and b),(4.12), and (4.25) we can write our system of ODEs in the form

$$\mathbf{V}' = f(t, \mathbf{V}; \mathbf{p}), \mathbf{V} \in \mathbb{R}^6, \mathbf{f} \in \mathbb{R}^6 \tag{5.3}$$

where $V_1 = V$ is the membrane voltage, $V_2 = [cGMP]$ is the cGMP concentration, $V_3 = [R]$ is the resact concentration, $V_4 = n$ is the KCNG gating variable, $V_5 = r$ is the HCN gating variable, and $V_6 = [Ca^{2+}]_{in}$ is the internal calcium concentration. In this form, we can apply the parameter

estimation techniques described in section 3.2.

We will determine parameters that allow us best to fit the base case; that is, the unstimulated pathway. In this state, the sperm cell maintains resting membrane voltage V_r and internal calcium concentration $[Ca^{2+}]_r$. Thus, the cost function we want to minimize is given by

$$\mathcal{F} = \sum [(V_r - V_1(t))^2 + ([Ca^{2+}]_r - V_6(t))^2]$$

This process gives us the parameters shown in Table 5.1. The remaining parameters can be found in Tables B.1 and B.2.

Table 5.1: Estimated Parameters

parameter	meaning	literature value	estimate
$\bar{g}_{KCNG}$ [nS]	KCNG max conductance	0.11 [8]	1.1
c_n [ms^{-1}]	KCNG activation rate constant	0.180 [5] (rock crab neuron)	1
$\bar{g}_{HCN}$ [nS]	HCN max conductance	4.8 [3](goldfish retina)	0.09
c_r [ms^{-1}]	HCN activation rate constant	0.00033 [5] (rock crab neuron)	1
V_r [mV]	HCN steady state half–max potential	-70 "	-200
s_r [mV]	HCN steady state step width	7 "	68
V_{kr} [mV]	HCN activation half–max potential	-110 "	-100
s_{kr} [mV]	HCN activation step width	-13 "	-7
$\bar{g}_{VOCC}$ [nS]	VOCC max conductance	0.046842 [9](rat uterus)	0.542
i_{PMCA} [pA]	PMCA max current	5.37 [3](goldfish retina)	7.249
i_{NCX} [pA]	NCX max current	5 [3](goldfish retina)	1.5

The code we use allows for the introduction of resact after a time delay. Introducing resact in this way is akin to "activating" the signaling pathway and we can see how the system changes when stimulated. First, we tried the base case, when the sperm is unstimulated. As seen in Fig. 5.6, the unstimulated membrane voltage stays constant and is close to the theoretical value. In addition, the calcium concentration remained at close to the resting calcium level $[Ca^{2+}]_r$. Hence, our model represents the base case accurately.

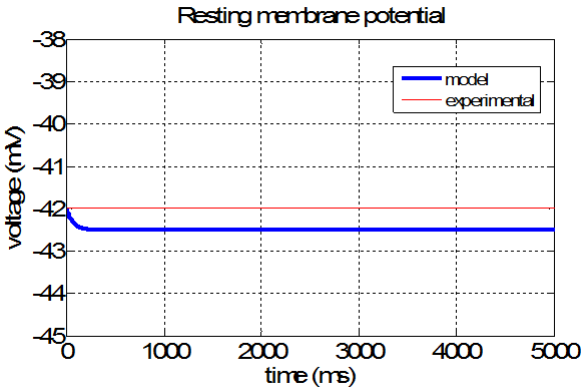

Figure 5.6: The inactive system remains at resting membrane voltage, achieved by parameter estimation

We then "activate" the system by introducing a small concentration of resact at 1000ms. The

resact increases cGMP concentration, which in turn contributes to the KCNG current, which finally changes the voltage. The resulting membrane voltage time course is shown in Fig. 5.7.

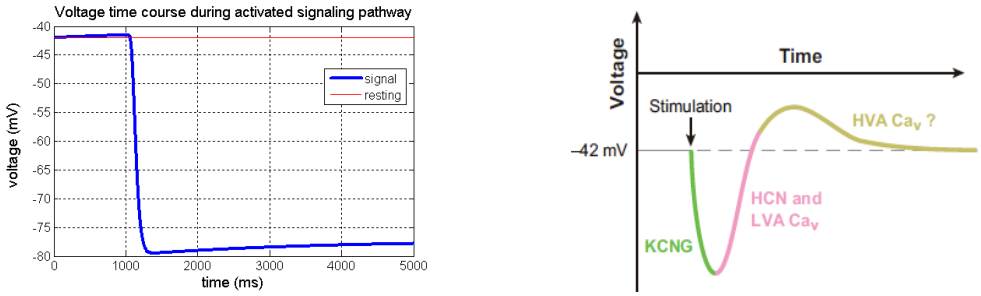

(a) (b)

Figure 5.7: Comparison between "activated" and ODE system voltage time course and expected voltage time course by [21]. In (a) we see the simulation results and in (b) the expected results.

We see that the voltage remains fairly closed to the expected resting potential before stimulation. After stimulation at 1000ms, The voltage drops to about −80mV due to the KCNG activity (Fig. 5.8a). However, beyond this point our model does not behave as expected. Our model does not depict the expected depolarization due to HCN activity shown in Fig. 5.7b. For a closer look at channel behavior, we show the time course for the major currents.

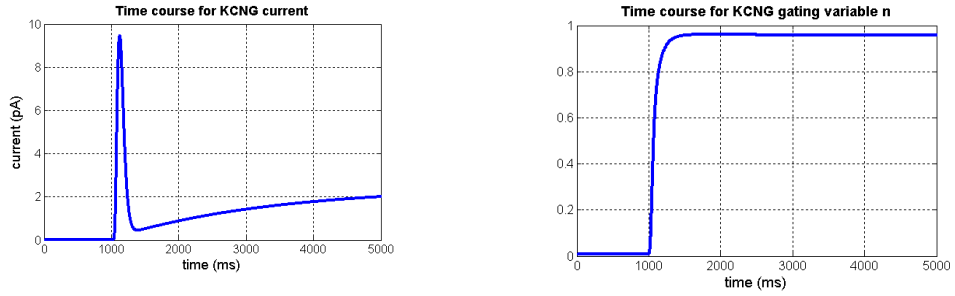

(a) (b)

Figure 5.8: The time course of the KCNG channel behavior when the system is stimulated by resact at 1000ms. In (a) we see the KCNG current and in (b) the channel gating.

Fig. 5.8 shows the behavior of equations (4.4) and (4.5), describing KCNG current and gating, respectively. Fig. 5.8a shows that the KCNG current is zero while the systsem is unstimulated. This represents the fact that the channel is closed when the sperm is at rest. When resact is introduced, the KCNG channel spikes positively for a 200ms duration, after which it returns to base current value and slowly increases over time. This corresponds to it letting a positive current out of the cell, which is the desired outcome. From Fig. 5.8b, we see the gating activation of the KCNG remains very high (almost all channels are open) over the time period, which results in the slow current increase over time and violates our expectations that the KCNG channel should deactivate after it spikes.

Fig. 5.9 shows the behavior of equations (4.11) and (4.12), describing HCN current and gating, respectively. As is the case with KCNG, Fig. 5.9a shows that the HCN current is zero while the system is unstimulated. This represents the fact that the channel is closed when the sperm is at rest. When resact is introduced, the I_{HCN} slowly decreases. This corresponds to it letting a negative current into the cell, which is the desired outcome. However, the rate of decrease is too slow—due

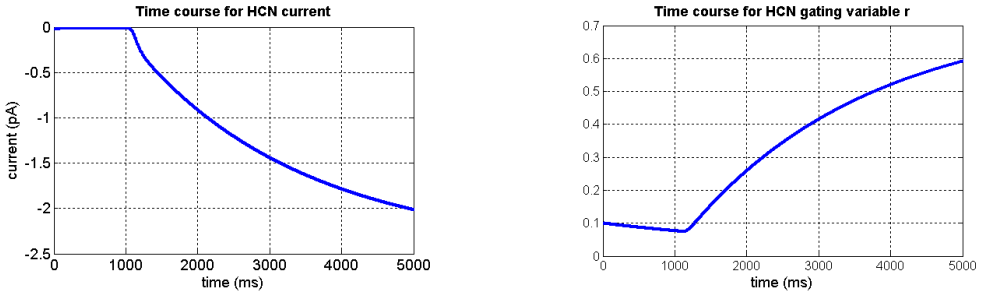

(a) (b)

Figure 5.9: The time course of the HCN channel behavior when the system is stimulated by resact at 1000ms. In (a) we see the HCN current and in (b) the channel gating.

to slow increase in gating activation in Fig. 5.9b—to affect the membrane voltage in the desired way (depolarization).

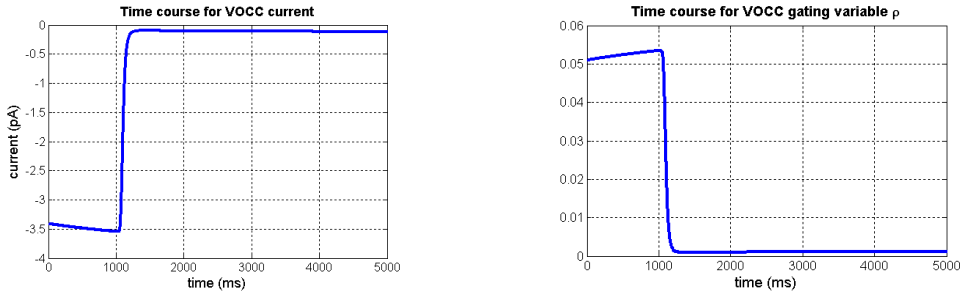

(a) (b)

Figure 5.10: The time course of the VOCC channel behavior when the system is stimulated by resact at 1000ms. In (a) we see the VOCC current and in (b) the channel gating.

Fig. 5.10 shows the behavior of equations (4.18) and (4.19), describing VOCC current and gating, respectively. Unlike the case with KCNG and HCN, Fig. 5.9a shows that the VOCC is active even while the systsem is unstimulated, with I_{VOCC} at about -3.5pA. This represents the fact that the channel is open and letting Ca^{2+} ions into the cell. When the system is stimulated by resact, I_{VOCC} increases to 0pA, that is, the VOCC channel closes. This is reflected in the gating mechanics shown in Fig. 5.10b, where we see the gating activation of the VOCC starts high and then decreases to zero when resact is introduced. This is the opposite of what we desire: that I_{VOCC} remains zero when the system is at rest and becomes more active (negative) when the system is stimulated.

Fig. 5.11 shows the behavior of calcium flux (equation (4.25)). In accordance with the VOCC dynamics shown in Fig. 5.10, the internal calcium concentration slightly increases before the system is stimulated by resacted, then decreases to 0 after stimulation. The decrease in concentrations occurs because of the action of the NCX and PMCA channels, with fluxes J_{NCX} and J_{PMCA} respectively, removing internal calcium ions. Again, this is the opposite of the desired outcome.

5.2.1 Isolating the Equations

For insight into the behavior of the current equations, we solve the ODE system with the same resact delay, though considering only the action of a single channel on the voltage. For example if we consider only the KCNG current in equation (4.1), we get the results shown in Fig. 5.12.

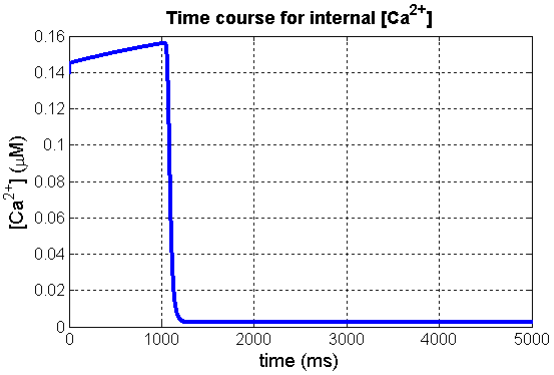

Figure 5.11: The time course of the internal calcium concentration when the system is stimulated by resact at 1000ms.

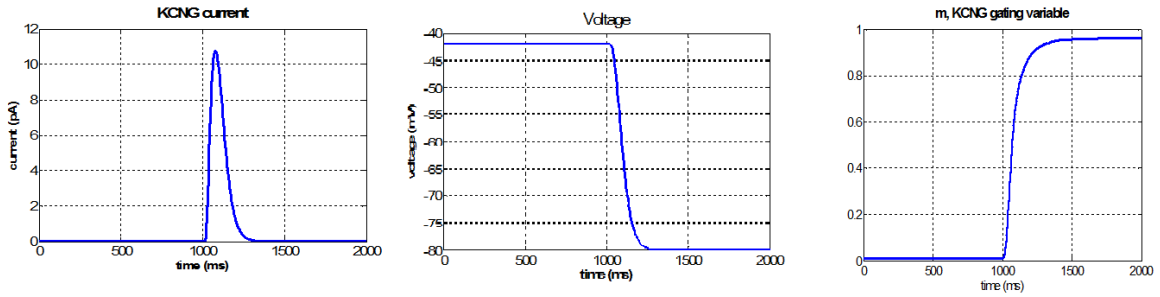

(a) **(b)** **(c)**

Figure 5.12: Isolated KCNG results with cGMP introduced at 1000ms, with all other currents set to zero. (a) shows the current, (b) shows the voltage response, and (c) shows the channel gating.

Fig. 5.12a shows the KCNG current behaving as we desire: it is zero while the system is unstimulated, spikes when stimulated by resact, and quickly decreases back to zero once hyperpolarization is achieved. In Fig. 5.12b, the voltage hyperpolarization levels off at -80mV because that is the Nernst potential of KCNG (Table B.2). At this membrane potential, there is no KCNG current, and thus no change in voltage. The gating variable m remains at a high proportion even though there is no KCNG current, as shown in Fig. 5.12c. This high activation proportion is responsible for the lack of depolarization in Fig. 5.7a: KCNG dominates the effects that the HCN current has on the membrane potential.

We repeat for the HCN channel, though this time we apply an external current with a step function of magnitude 10pA for 200ms at the 1000ms time mark to stimulate the system. This current is used to mimic the hyperpolarization caused by the KCNG channel, since the HCN channel has no direct dependence on cGMP concentration. As is the case with the isolated KCNG channel, Fig. 5.13a shows the HCN current behaving as we desire: it is zero while the system is unstimulated, spikes negatively when stimulated by resact, and quickly increases back to zero, depolarizing the cell in the process (Fig. 5.13b). The voltage depolarization levels off at -40mV because that is the Nernst potential of HCN (Table B.2). From Fig. 5.13c, the gating variable r increases when the system is stimulated at 1000ms, and then decreases as depolarization is achieved. This is the behavior we expect.

Finally, we solved the system of ODEs considering all the currents in equation (4.1) except for

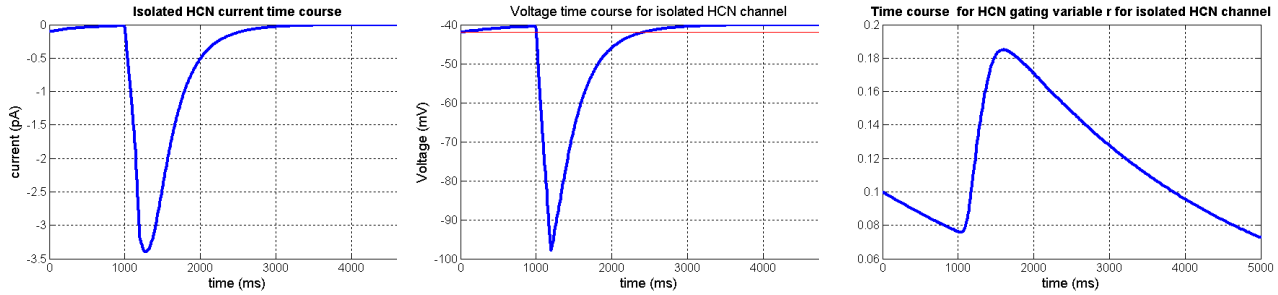

(a) **(b)** **(c)**

Figure 5.13: Isolated HCN results with an applied current introduced at 1000ms, with all other currents set to 0. (a) shows the current, (b) shows the voltage response, and (c) show the channel gating.

the KCNG current, using the same externally applied current described above in its place. We found that the HCN channel behaved in the same manner as depicted in Fig. 5.13. In addition, the calcium mechanics can be seen in Fig. 5.14.

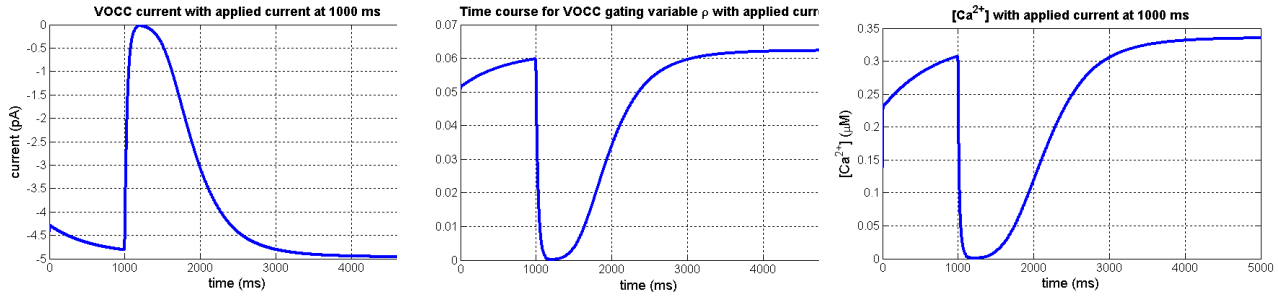

(a) **(b)** **(c)**

Figure 5.14: VOCC results with an applied current introduced at 1000ms instead of a cGMP current. (a) shows the current, (b) shows the voltage response, and (c) shows the channel gating.

From Fig. 5.14a, the VOCC is still active before the system is stimulated and still decreases in activity once the system is stimulated. However, the figure also shows that the VOCC channel reactivates as the membrane is depolarized, which is biologicaly accurate. The gating variable ρ does not deactivate (Fig. 5.14b), thus steadily increasing internal Ca^{2+} concentration (Fig. 5.14c). This is biologically inaccurate and undesirable (see Sec. 2.4.1).

5.2.2 Gating Kinetics

The source of the main problem with our model seems to be the gating of the KCNG, HCN, and VOCC channels; they retain high activation rates when we desire them not to. To understand why the current equations for these channels behave the way they do, we can perform steady state analysis on their corresponding gating variables.

KCNG Channel The gating variable n for the KCNG channel satisfies the differential equation

$$\frac{dn}{dt} = [n_\infty(V_m) - n]k_n(V_m) \ . \tag{5.4}$$

Thus, at steady state activation ($\frac{dn}{dt} = 0$), we have

$$n = n_\infty = \frac{1}{\left(1 + \exp\left(\frac{V - V_n}{s_n}\right)\right)} \left(\frac{[cGMP]^H}{K_{cGMP}^H + [cGMP]^H}\right)$$

as a function of voltage.

Doing the same for the gating variable r for the HCN channel, we get

$$r = r_\infty = \frac{1}{\left(1 + \exp\left(\frac{V - V_{kr}}{s_{kr}}\right)\right)} .$$

Fig. 5.15a shows how the steady activation of the KCNG channel, with [cGMP] set to zero, responds to voltage.

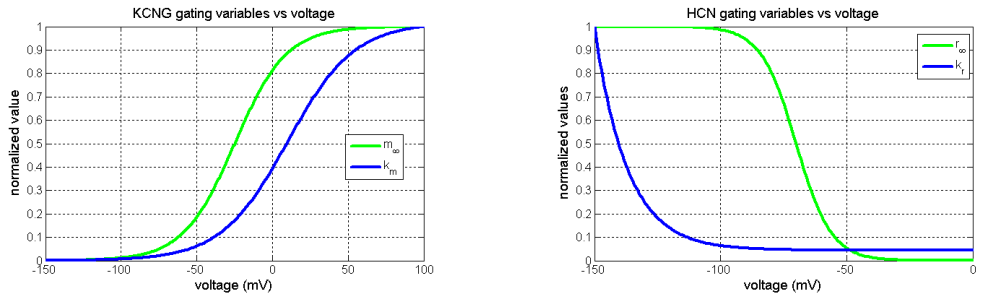

(a) (b)

Figure 5.15: Gating kinetics of the KCNG channel. (a) shows the how the KCNG steady state activation and activation rates change with voltage, and (b) shows the same for the HCN gating variables.

The activation of the KCNG channel by cGMP causes the membrane voltage to become more negative. We can see, from Fig. 5.15a, that the steady state activation is relatively high at around $V = -42$mV ($n_\infty \approx 0.4$), causing the KCNG to activate. As the membrane voltage decreases (hyperpolarization) due to KCNG activity, n_∞ tends to zero. This means the KCNG is deactivated at more negative membrane potentials (at about -80mV), which is biologically accurate. Hyperpolarization yields high HCN activity, as can be seen by the steady state activation r_∞ in Fig. 5.15b. Therefore, HCN activity is stimulated by hyperpolarization, as desired. The HCN channel increases membrane voltage (depolarization), which according to Fig. 5.15a mathematically reactivates the KCNG channel. Biologically, however, this reactivation should be mitigated by lowered cGMP concentrations. This is not shown in Fig. 5.8a, in which there is a slow but steady rise in KCNG current after the HCN is activated. This implies that the model should include either a new form of cGMP dependence to more accurately recreate the mitigation in KCNG current caused by low cGMP concentration or a separate inactivation gating variable that inactivates the channel as voltage increases.

From Fig. 5.16, the VOCC channel is active at depolarized membrane voltages, which is desired from the biological description of the signaling pathway. However, this activation occurs regardless of stimulation of the system by cGMP (Fig. 5.10a) which is not kosher. This again implies that the model may be missing either a second messenger dependence or a separate inactivation gating variable for the VOCC channel that renders the channel inactive until the system is stimulated by resact.

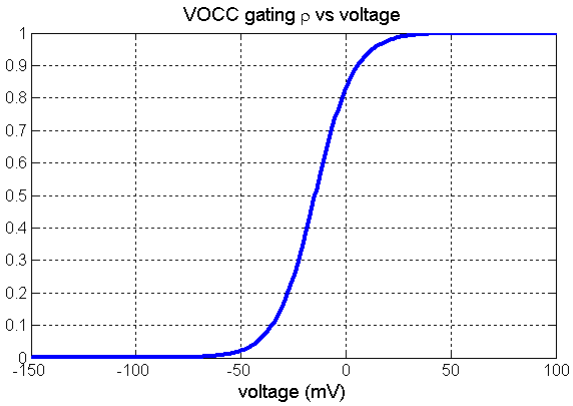

Figure 5.16: Gating kinetics of the VOCC channel. The steady state activation of VOCC changes with voltage,

Chapter 6

Discussion

Sea urchin sperm move by chemotaxis to find the egg.. The sea urchin egg releases a protein called resact which, when binded to the sperm tail, sparks a signaling pathway that results in calcium influx into the cell. This calcium influx is what causes sperm to change their swimming trajectory in the direction of the egg. The signaling process involves changes in membrane voltage cause by ion channels—in particular, the KCNG channel, the HCN channel, and the VOCC channel. The KCNG channel, the first channel in the pathway depends on a second messenger of resact called cGMP to start the process. Thus, the influx of calcium, and the trajectory of the sperm, depend on changes in membrane voltage and ion currents.

A mathematical model that describes this signaling process and the interaction between these channels has never been attempted before. We proposed a model based on Hodgkin–Huxley ion channel mechanics, taking inspiration from the similar works of other biologists and mathematicians. We applied parameter estimation techniques where appropriate to ensure the model correctly described the unstimulated (base) case of the signaling pathway (constant membrane voltage and internal calcium concentration).

When the system is stimulated, we see that the model behaves correctly regarding some of the biological aspects of the signaling process (membrane hyperpolarization upon stimulation), and incorrectly regarding others (no membrane depolarization when expected). We studied these problems by observing the behaviors of each current in isolation, and by analyzing the gating activation variables of these channels. Our results indicate there may be other ion channels or second messengers that contribute to the signaling process that are not included in our model. Our results also indicate the possibility that gating inactivation variables are necessary to more accurately capture this biological phenomenon. We suggest future research along these lines.

Appendix A

Units

Below is a table describe the units for each quanitity we use.

Table A.1: Units

Quantity	units	comments
Voltage	mV	
Current	pA	
Conductance	nS	conversion: $[S] = \left[\frac{A}{V}\right]$ and so $[nS] = \left[\frac{pA}{mV}\right]$
Capacitance	pF	conversion: $[F] = \left[\frac{A \times s}{V}\right]$ and so $[pF] = \left[\frac{pA \times ms}{mV}\right]$
Concentration	μM	
Time	ms	
Flux	$\mu\text{M} \times \text{ms}^{-1}$	
Volume	dm^3	

Equations

We show that these units are balanced in out equations

- **Currents**: the typical current equation is $I_{ion} = g_{ion}(V - E_{ion})m$
- Unit equation
$$\left[\frac{pA \times mV}{mV}\right] = [pA]$$
- **Voltage**: we have $C_m \frac{dV}{dt} = -\Sigma(I_{ion})$
- Unit equation
$$\left[\frac{pF \times mV}{ms}\right] = \left[\frac{pA \times ms}{mV}\frac{mV}{ms}\right] = [pA]$$
- **Calcium flux**: we describe our calcium flux by $J_{ion} = \frac{I_{ion}}{2F \times Vol}$ (F here is Faraday's constant, with units C/mol)

- If we change the units of Faraday's constant:

$$\left[\frac{C}{mol}\right] = \left[\frac{A \times s}{mol}\right] = \left[\frac{pA \times ms}{\mu mol}\frac{10^{15}}{10^{6}}\right]$$

then we get

$$\left[\frac{pA \times \mu mol}{m^3 \times pA \times ms}10^{-9}\right] = \left[\frac{\mu mol}{m^3 \times ms}10^{-9} = \frac{\mu M}{ms}10^{-9}\right]$$

and so, using our units, our flux should be described by $J_{ion} = \frac{I_{ion}}{2F \times Vol}10^{-9}$

- **Reversal potential**: The reversal potential of an ion channel is defined by $E_{ion} = \frac{RT}{2F} ln\left(\frac{[ion]_{in}}{[ion]_{out}}\right)$ which has unit equation

$$\left[\frac{mJ \cdot mol \cdot K}{mol \cdot K \cdot C}\right] = \left[\frac{mJ}{C}\right] = [mV]$$

.

Appendix B

Parameters

Below is a table of parameters used in the equations above, including the type of cell in which they've been measured.

Table B.1: General Parameters

Misc Parameters			
R [mJmol^{-1}K^{-1}]	Ideal gas constant	8341	[9](rat uterus)
T [K]	temperature	310	"
F [Cmol^{-1}]	Faraday constant	96487	"
	Calcium valence	2	
	Sperm tail volume	$45\pi\times10^{-15}$ [dm^3]	estimated from [11]
C_m	Membrane capacitance [pF]	30	[31] (rat neuron)
V_r	Sperm resting membrane potential [mV]	-42	[21]
$[Ca^{2+}]_r$	Sperm resting calcium concentration [nM]	0.14	[21]

Table B.2: Computational parameters for calcium dynamics

KCNG Channel	meaning	value	reference
$\bar{g}_{KCNG}$ [nS]	KCNG max conductance	1.1	estimated
		0.11	[8](sea urchin sperm)
E_{KCNG} [mV]	KCNG reversal potential	-80	[8](sea urchin sperm)
KCNG gating activation, n			
c_n [ms^{-1}]	rate constant	1	estimated
V_n [mV]	half-maximal potential of n_∞	-25	[5]
s_n [mV]	step width of n_∞	17	"
V_{kn} [mV]	half-maximal potential of k_n	10	"
s_{kn} [mV]	step width potential of k_n	-22	"
cGMP Mechanics			
q_1 [mV]	cGMP synthesis rate	0.0147	estimated
q_2 [mV]	cGMP degradation rate	0.7432	estimated
q_3 [mV]	cGMP Michaelis constant	1693.2422	estimated
q_4 [mV]	resact degradation rate	0.0012	estimated
HCN Channel			
$\bar{g}_{HCN}$ [nS]	HCN max conductance	0.09	estimated
E_{HCN} [mV]	HCN reversal potential	-40	[8](sea urchin sperm)
HCN gating activation, r			
c_r [ms^{-1}]	rate constant	1	estimated
V_r [mV]	half-maximal potential of r_∞	-200	[5]
s_r [mV]	step width of r_∞	68	"
V_{kr} [mV]	half-maximal potential of k_r	-100	"
s_{kr} [mV]	step width of k_r	-7	"
VOCC Channel	meaning	value	reference
$\bar{g}_{VOCC}$ [nS]	LVOCC max conductance	0.242	estimated
VOCC gating activation, ρ			
V_ρ [mV]	Half–maximal potential	-14.8	"
s_ρ [mV]	step width of ρ	9.3	"
PMCA Channel			
i_{PMCA} [pA]	PMCA max current	5.37	[3](goldfish retina)
K_{PMCA} [μM]	M–M dissociation constant	0.17	"
NCX Channel			
i_{NCX} [pA]	NCX max current	5	[3](goldfish retina)
V_λ	Half–maximal potential	-14	[3](goldfish retina)
s_λ	step width of λ	70	[3](goldfish retina)

Appendix C

Code

C.1 Interpolation

```
function a=interpcgmp(r)
%
% Spline interpolation of cGMP data from Kaupp
%
% input: resact concentration = r
%
% output: cubic spline polynomial interpolant = a
%
%

vol=pi*43.3e-15; %volume of sperm cell in dm^3

% Reads cGMP concentration data dependent on resact concentration.
switch r
    case 0.25
        data=xlsread('NoIBMXpt25.xls');

    case 2.5
        data=xlsread('NoIBMX2pt5.xls');

    case 25
        data=xlsread('NoIBMX25.xls');

    case 250
        data=xlsread('NoIBMX250.xls');

    otherwise
        a=0;
end

x=1000*data(:,1); %converts units of time data from s to ms
raw=data(:,2);
y=raw*1e-8*(1e-6)/vol; %converts raw data from pmol/10^8 cells to uM in a single cell.
```

```
a=pchip(x,y); %interpolates data and stores as piecewise polynomial.
```

C.2 Parameter Optimization

```
% optimizeSD: Uses NelderMead optimization routine with cost function costfunccgmp
% to determine the best parameters to fit the ODE cgmpDynamPE to one set of cGMP data
function optimizeSD

global optparams iterations Jmin Variance ICs tspan
CalModParam;

ICs    = [-42;0.01;0.14;0.1]; %Initial conditions
tspan  = [0 2000]; %Start and end time
params = [cr g_hcn -V_half K_half 14 3]; %Parameters for code to optimize
params = sqrt(params);  %taking square root to send to simpgen.m, which is necessary to find
%contraction/shrinkage, etc for the simplex vertices for nelder mead algorithm
%Note that in costfuncSD.m file, parameters are squared

%these next three lines are necessary for the cost function using nelder mead optimization
Jmin = 1000;
optparams  = zeros(length(params),1);
iterations = 0;

%data = load('Data'); %this loads the noisy data created in the createdata.m file
%Since error will be based just on difference between resting voltage and
%ODE solved voltage, we will define 'data' or resting voltage in the cost
%function

%simpgen function creating the contraction/shrinkage,... for nelder mead
V0 = simpgen(params); %this is necessary for the costfunction/optimization

%this is calling the nelder optimization
[X,lhist,histout,simpdata] = nelder(V0,'costfuncSD',1e-6, 2000, 2000);
%nelder(V0,'costfunc',1e-6, 2000, 2000);
%V0=vertices of initial simplex (x0 in nelder.m)
%'costfunc'=an m file that calculates the cost or error between ODE solver
%value and resting voltage that you want (f in nelder.m)
%1e-6=tolerance, if error is less than this value, optimization routine
%ends
%2000=maxit= maximum number of times to run through nelder optimization
%if it runs 2000 times and error does not decrease, need better initial
%guesses parameters
%2000=budget=maximum number of times to evaluate the cost (error) function
optparams
iterations
Jmin
Variance

%creating new parameter vector q with each iteration of optimization
%using optimized parameters found
q = optparams
```

C.2.1 Cost Function

Cost function for optimizeSD.

```
%costfuncSD: The cost function for optimizeSD featuring both Voltage and
%calcium concentration

function  J = costfuncSD(params)

global optparams iterations Jmin Variance ICs tspan

params = params.^2;

iterations = iterations + 1;

q    = params

ODEopt=odeset('reltol',1e-6,'abstol',1e-6);
[tdata xdata]=ode45(@SDkcnghcngatePE,tspan,ICs,ODEopt,q);


%the length of the timed vector is the number of time points being used in cost function
N  = length(tdata)
RestVolt=ICs(1)*ones(N,1);
RestCalc=ICs(3)*ones(N,1);
VoltODE=xdata(:,1);
CalcODE=xdata(:,3);

%This calculates the cost J
J=0;
for i=1:N
    J=J+(RestVolt(i)-VoltODE(i))^2 +(RestCalc(i)-CalcODE(i))^2;
end
J=J/N;
%J = sum((RestVolt-VoltODE).^2)/N
display(J)
%This calculates the variance needed for later to do confidence intervals
%check to see if the J/(N-#) has that the #=number of parameters estimated
Variance = J/(N-6);
if(J < Jmin)
    Jmin = J;
    optparams = params;
end
```

C.2.2 Nelder-Mead Optimization

```
function [x,lhist,histout,simpdata]=nelder(x0,f,tol,maxit,budget)
%
% Nelder-Mead optimizer, No tie-breaking rule other than MATLAB's sort
%
% C. T. Kelley, December 12, 1996
%
%
% This code comes with no guarantee or warranty of any kind.
%
% function [x,lhist,histout,simpdata] = nelder(x0,f,tol,maxit,budget)
%
% inputs:
% vertices of initial simplex = x0 (n x n+1 matrix)
%          The code will order the vertices for you and no benefit is
%          accrued if you do it yourself.
%
%       objective function = f  ( calling the cost function  )
%
%       termination tolerance = tol
%       maximum number of iterations = maxit (default = 100)
%           As of today, dist = | best value - worst value | < tol
%           or when maxit iterations have been taken
%       budget = max f evals (default=50*number of variables)
%                 The iteration will terminate after the iteration that
%                 exhausts the budget
%
%
% outputs:
% final simplex = x (n x n+1) matrix
%
%       number of iterations before termination = itout (optional)
%       iteration histor = histout itout x 5
%         histout = iteration history, updated after each nonlinear iteration
%                 = lhist x 5 array, the rows are
%                   [fcount, fval, norm(grad), dist, diam]
%                   fcount = cumulative function evals
%                   fval = current best function value
%                   norm(grad) = current simplex grad norm
%                   dist = difference between worst and best values
%                   diam = max oriented length
%       simpdata = data for simplex gradient restart
%              = [norm(grad), cond(v), bar f]
%
% initialize counters
%
lhist=0; fcount=0;
%
% set debug=1 to print out iteration stats
```

```
%
debug=0;
%
% Set the N-M parameters
%
rho=1; chi=2; gamma=.5; sigma=.5;
dsize=size(x0); n=dsize(1);
if nargin < 4 maxit=100; end
if nargin < 5 budget=100*n; end
%
% set the paramters for stagnation detection/fixup
% setting oshrink=0 gives vanilla Nelder-Mead
%
oshrink=1; restartmax=3; restarts=0;
%
%
% Order the vertices for the first time
%
x=x0; [n,m]=size(x); histout=zeros(maxit*3,5); simpdata=zeros(maxit,3);
itout=0; orth=0;
xtmp=zeros(n,n+1); z=zeros(n,n); delf=zeros(n,1);
for j=1:n+1; fv(j)=feval(f,x(:,j)); end; fcount=fcount+n+1;
[fs,is]=sort(fv); xtmp=x(:,is); x=xtmp; fv=fs;
itc=0; dist=fv(n+1)-fv(1);
diam=zeros(n,1);
for j=2:n+1
   v(:,j-1)=-x(:,1)+x(:,j);
   delf(j-1)=fv(j)-fv(1);
   diam(j-1)=norm(v(:,j-1));
end
sgrad=v'\delf; alpha=1.d-4*max(diam)/norm(sgrad);
lhist=lhist+1;
histout(lhist,:)=[fcount, fv(1), norm(sgrad,inf), 0, max(diam)];
%
% main N-M loop
%
while(itc < maxit & dist > tol & restarts < restartmax & fcount <= budget)
    fbc=sum(fv)/(n+1);
    xbc=sum(x')'/(n+1);
    sgrad=v'\delf;
    simpdata(itc+1,1)=norm(sgrad);
    simpdata(itc+1,2)=cond(v);
    simpdata(itc+1,3)=fbc;
    if(det(v) == 0)
        disp('simplex collapse')
        break
    end
    happy=0; itc=itc+1; itout=itc;
%
```

```
% reflect
%
    y=x(:,1:n);
    xbart = sum(y')/n;  % centriod of better vertices
    xbar=xbart';
    xr=(1 + rho)*xbar - rho*x(:,n+1);
    fr=feval(f,xr); fcount=fcount+1;
    if(fr >= fv(1) & fr < fv(n)) happy = 1; xn=xr; fn=fr; end;
%    if(happy==1) disp(' reflect '); end
%
% expand
%
    if(happy == 0 & fr < fv(1))
        xe = (1 + rho*chi)*xbar - rho*chi*x(:,n+1);
        fe=feval(f,xe); fcount=fcount+1;
        if(fe < fr) xn=xe;  fn=fe; happy=1; end
        if(fe >=fr) xn=xr;  fn=fr; happy=1; end
%        if(happy==1) disp(' expand '); end
    end
%
% contract
%
   if(happy == 0 & fr >= fv(n) & fr < fv(n+1))
%
% outside contraction
%
       xc=(1 + rho*gamma)*xbar - rho*gamma*x(:,n+1);
       fc=feval(f,xc); fcount=fcount+1;
       if(fc <= fr) xn=xc; fn=fc; happy=1; end;
%       if(happy==1) disp(' outside '); end;
   end
%
% inside contraction
%
   if(happy == 0 & fr >= fv(n+1))
       xc=(1 - gamma)*xbar+gamma*x(:,n+1);
       fc=feval(f,xc); fcount=fcount+1;
       if(fc < fv(n+1)) happy=1; xn=xc; fn=fc; end;
%   if(happy==1) disp(' inside '); end;
   end
%
%  test for sufficient decrease,
%  do an oriented shrink if necessary
%
   if(happy==1 & oshrink==1)
       xt=x; xt(:,n+1)=xn; ft=fv; ft(n+1)=fn;
%       xt=x; xt(:,n+1)=xn; ft=fv; ft(n+1)=feval(f,xn); fcount=fcount+1;
       fbt=sum(ft)/(n+1); delfb=fbt-fbc; armtst=alpha*norm(sgrad)^2;
       if(delfb > -armtst/n)
```

```
            restarts=restarts+1;
            orth=1; diams=min(diam);
            sx=.5+sign(sgrad); sx=sign(sx);
if debug==1
            [itc, delfb, armtst]
end
            happy=0;
            for j=2:n+1; x(:,j)=x(:,1);
            x(j-1,j)=x(j-1,j)-diams*sx(j-1); end;
        end
    end
%
%  if you have accepted a new point, nuke the old point and
%  resort
%
    if(happy==1)
        x(:,n+1)=xn; fv(n+1)=fn;
%        x(:,n+1)=xn; fv(n+1)=feval(f,xn); fcount=fcount+1;
        [fs,is]=sort(fv); xtmp=x(:,is); x=xtmp; fv=fs;
    end
%
% You're in trouble now! Shrink or restart.
%
    if(restarts >= restartmax) disp(' stagnation in Nelder-Mead'); end;
    if(happy == 0 & restarts < restartmax)
        if(orth ~=1) disp(' shrink '); end;
        if(orth ==1)
        if debug == 1 disp(' restart '); end
        orth=0; end;
        for j=2:n+1;
            x(:,j)=x(:,1)+sigma*(x(:,j)-x(:,1));
            fv(j)=feval(f,x(:,j));
        end
        fcount=fcount+n;
        [fs,is]=sort(fv); xtmp=x(:,is); x=xtmp; fv=fs;
    end
%
%  compute the diameter of the new simplex and the iteration data
%
    for j=2:n+1
        v(:,j-1)=-x(:,1)+x(:,j);
        delf(j-1)=fv(j)-fv(1);
        diam(j-1)=norm(v(:,j-1));
    end
    dist=fv(n+1)-fv(1);
    lhist=lhist+1;
    sgrad=v'\delf;
    histout(lhist,:)=[fcount, fv(1), norm(sgrad,inf), dist, max(diam)];
end
```

C.2.3 Simplex generation

Generates simplex for `nelder`.

```
function V0 = simpgen(x0)

dim = length(x0);
if size(x0,1) == dim
    vertex = x0;
elseif size(x0,2) == dim
    vertex = x0';
else
    error('Houston, we have a problem: Initial vertex has spring a leak');
end

p = (dim-1+sqrt(dim+1))/dim/sqrt(2);
q = (sqrt(dim+1)-1)/dim/sqrt(2);
D = toeplitz([p q*ones(1,dim-1)]);
V  = [vertex D];
V0 = [V(:,1) V(:,2:dim+1)+repmat(V(:,1),1,dim)];
```

Bibliography

[1] J Adler. Chemotaxis in bacteria. *Science*, 153(3737):708–716, 1966.

[2] L Alvarez, L Dai, BM Friedrich, ND Kashikar, I Gregor, R Pascal, and UB Kaupp. The rate of change in ca^{2+} concentration controls sperm chemotaxis. *J Cell Biol*, 196(5):653–663, 2012.

[3] T Aoyama, Y Kamiyama, and S Usui. Simulation analysis of receptive-field size of retinal horizontal cells by ionic current model. *Visual Neuroscience*, 22:65–78, 2005.

[4] Alberts B, Johnson A, and Lewis J. *Molecular Biology of the Cell*. Garland Science.

[5] F buchholtz, J Golowasch, I Epstein, and E Marder. Mathematical model of an identified stomatogastric ganglion neuron. *J Neurophysiol*, 67(2):332–340, 1992.

[6] K Craven and W Zagotta. Cng and hcn channels: Two peas, one pod. *Annu Rev Physiol*, 66:375–401, 2006.

[7] A Cukkemane, R Seifert, and UB Kaupp. Cooperative and uncooperative cyclic-nucleotide-gated ion channels. *Trends in Biochemical Sciences*, 36(1):55–63, 2011.

[8] A Darszon, V Vacquier, P Labarca, B Galindo, and JL de la Vega-Beltran. Sp-tetrakcng: A novel cyclic nucleotide gated k^+ channel. *Biochemical and Biophysical Research Communications*, 354:668–675, 2007.

[9] D Elad, A Jaffa, O Eytan, and L Bursztyn. Mathematical model of excitation-contraction in a uterine smooth muscle cell. *Am J Physiol Cell Physiol*, 292(5):C1816–C1829, 2007.

[10] UNSW Embryology. Spermatozoa development. `http://php.med.unsw.edu.au/embryology/index.php?title=Spermatozoa_Development`, November 2012.

[11] D Eshel, C Shingyoji, K Yoshimura, B Gibbons, I Gibbons, and K Takahashi. Transient behavior of sea urchin sperm flagella following an abrupt change in beat frequency. *J exp Bio*, 152:441–451, 1990.

[12] E Fong, J Kim, and A Lin. Mitosis in sea urchin embryos. `http://www.rpgroup.caltech.edu/courses/aph162/2006/webpages/Projects/Alex-JinHong-Eileen/seaurchins.html`, July 2006.

[13] goldiesroom.org. Cytology. `http://www.goldiesroom.org/Note\%20Packets/03\%20Cytology/00\%20Cytology--WHOLE.htm`, August 2008.

[14] H Gunaratne, A Neill, and V Vacquier. Plasma membrane calcium atpase is concentrated in the head of sea urchin spermatazoa. *J Cell Biol*, 207:413–419, 2005.

[15] A Hodgkin. The ionic basis of electrical activity in nerve and muscle. *Biol Rev*, 26:339–409, 1951.

[16] A Hodgkin and A Keynes. Active transport of cations in giant axons from sepia and loligo. *J Physiol*, 128:28–60, 1955.

[17] howMed.net. Action potential. `http://howmed.net/physiology/action-potential/`, July 2011.

[18] F Julicher and B Friedrich. Chemotaxis of sperm cells. *PNAS*, 104(33):13256–13261, 2007.

[19] A Kapela, A Bezerianos, and N Tsoukias. A mathematical model of ca^{2+} dynamics in rat mesenteric smooth muscle cell: Agonist and no stimulation. *Journal of Theoretical Biology*, 253:238–260, 2008.

[20] A Kapela, A Bezerianos, and N Tsoukias. Mathematical model of excitation-contraction in a uterine smooth muscle cell. *Journal of Theoretical Biology*, 253:238–260, 2008.

[21] UB Kaupp, ND Kashikar, and I Weyand. Mechanisms of sperm chemotaxis. *Annu Rev Physiol*, 70:93–117, 2008.

[22] Kohlasz. Chemotaxis-attractant-repellent. `http://en.wikipedia.org/wiki/File:Chtx-AttrRep-en.png`, 2008.

[23] M Kuramochi and Y Iwasaki. Quantitiative modeling of neuronal dynamics in *c. elegans*. pages 17–24, 2010.

[24] WR Lieb and WD Stein. *Transport and Diffusion across Cell Membranes*. San Diego: Academic Press.

[25] S Olson. Fluid dynamic model of invertebrate sperm chemotactic motility with varying calcium inputs. *J Biomech*, 46:329–337, 2013.

[26] MJD Powell. On search directions for minimization algorithms. *Mathematical Programming*, 4:193–201, 1973.

[27] DK Serafy. Echinoids (echinodermata: Echinoidea). *Mem. Hourglass Cruises*, 5:1–120, October 1979.

[28] J Sneyd and J Keener. *Mathematical Physiology*. Springer-Verlag.

[29] Y Su and V Vacquier. A flagellar k^+–dependent na^+/ca^{2+} exchanger keeps ca^{2+} low in sea urchin spermatazoa. *PNAS*, 99(10):6743–6745, 2002.

[30] SynaptitudeKohlasz. Diagram showing the ionic basis of the resting potentia. `http://en.wikipedia.org/wiki/File:Basis_of_Membrane_Potential2.png`, 2011.

[31] M Wechselberger, C Wright, G Bishop, and J Boulant. Ionic channels and conductance-based models for hypothalamic neuronal thermosensitivity. *Am J Physiol Regul Integr Comp Physiol*, 291(3):R518–R529, 2006.